# Palaeomagnetic and geochronological data from Late Mesoproterozoic redbed sedimentary rocks on the western margin of Kalahari craton

JENNIFER KASBOHM[1,3]*, DAVID A. D. EVANS[1], JOSEPH E. PANZIK[1], MANDY HOFMANN[2] & ULF LINNEMANN[2]

[1]*Department of Geology and Geophysics, Yale University, New Haven, CT 06520-8109, USA*

[2]*Museum of Mineralogy and Geology, Senckenberg Natural History Collections Dresden, Königsbrücker Landstrasse 159, D-01109 Dresden, Germany*

[3]*Present Address: Department of Geosciences, Princeton University, Princeton, NJ 08544, USA*

**Corresponding author (e-mail: jkasbohm@princeton.edu)*

**Abstract:** Redbeds of the Aubures Formation constitute the uppermost stratigraphic unit in the Mesoproterozoic Sinclair succession of southern Namibia. Aubures palaeomagnetic remanence vectors, held almost exclusively by hematite, document at least one geomagnetic polarity reversal in the stratigraphy, a positive intraformational conglomerate test indicating primary magnetization and greatest concentration of characteristic directions at 50–60% untilting, indicating that deformation was coincident with sedimentation. The new Aubures palaeomagnetic pole, at 56.4°N and 018.0°E with $A_{95} = 11.3°$, is located on the apparent polar wander path of the Kalahari craton, between poles of the 1110 Ma Umkondo igneous event and the *c.* 1090 Ma Kalkpunt redbeds of the Koras Group near Upington, South Africa. This distinctive concordance suggests that Aubures sediments have an age of approximately 1100 Ma, that the Sinclair region was probably part of Kalahari at that time and that the Aubures and Kalkpunt redbeds are broadly correlative. New laser-ablation inductively coupled plasma mass spectrometry detrital zircon results from the Aubures Formation, including a youngest age component (1108 ± 9 Ma) that is coincident with the Kalahari-wide Umkondo large igneous province, conform to this interpretation. Palaeomagnetism and geochronology of the Sinclair succession can provide kinematic constraints on the tectonic evolution of Kalahari as it approached other cratons in the growing Rodinia supercontinent.

The Kalahari craton, in southern Africa, is thought to have played an important role in the early Neoproterozoic Rodinia supercontinent reconstructions (Hoffman 1991), because it was affected by widespread *c.* 1.2–1.0 Ga events of the Namaqua–Natal orogen (Thomas *et al.* 1994) followed by *c.* 0.8–0.7 Ga rifting (Frimmel *et al.* 1996; Macdonald *et al.* 2010). The particular location and orientation of Kalahari within the Rodinia assemblage, however, has been debated (Hanson *et al.* 2004; Jacobs *et al.* 2008; Loewy *et al.* 2011; Li *et al.* 2013). Palaeomagnetism of Proterozoic rocks can provide important insights into global and regional continental reconstructions, as well as the behaviour of the ancient geomagnetic field. Along the western margin of the Kalahari craton in southern Namibia (Fig. 1), late Mesoproterozoic volcanic and sedimentary rocks of the Sinclair region are regionally exposed and preserved at subgreenschist metamorphic grade (Miller 2008), and thus amenable to palaeomagnetic study. Pioneering palaeomagnetic work in the Sinclair succession (Piper 1975) was limited to analysis of either the natural remanent magnetization (NRM) of the rocks, or limited blanket AF demagnetization to 1600 Oe. The present report is part of a broad-scale palaeomagnetic study of the Sinclair region, using modern methods of vector analysis and field stability tests, beginning with the youngest stratigraphic unit, the Aubures Formation. In addition, we supplement the palaeomagnetic work with detrital-zircon provenance analysis for constraints on sedimentary source regions and a maximum depositional age for that redbed unit.

## Geological setting

The western Mesoproterozoic margin of Kalahari craton, known as the Namaqua Province, contains several distinct terranes bounded by NW–SE dextral shear zones extending from central Namibia into western South Africa (Miller 2012). The present study area lies within the low-grade Konkiep Subprovince, located in south-central Namibia, between the largely buried Namaqua tectonic front to the NE and the Excelsior–Lord Hill Lineament

*From*: Li, Z. X., Evans, D. A. D. & Murphy, J. B. (eds) 2016. *Supercontinent Cycles Through Earth History*. Geological Society, London, Special Publications, **424**, 145–165.
First published online May 21, 2015, http://doi.org/10.1144/SP424.4

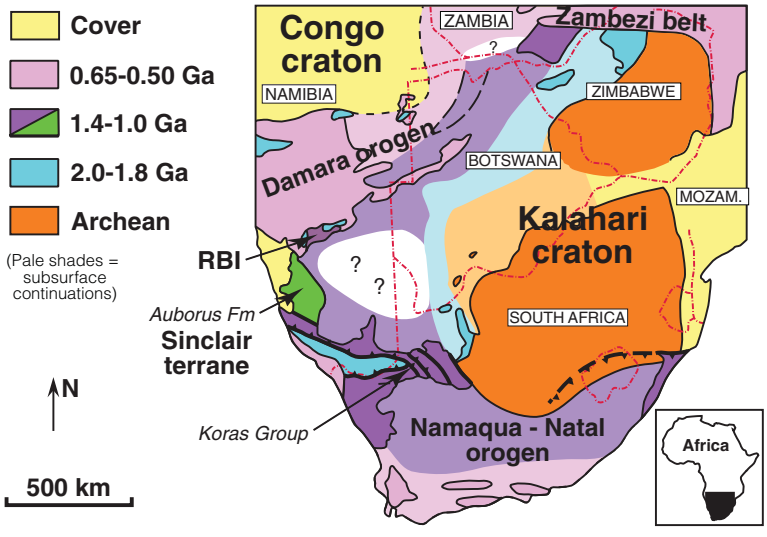


**Fig. 1.** Simplified tectonic map of southern Africa, modified from Hanson (2003). RBI, Rehoboth basement inlier.

to the SW. The Namaqua Front has been interpreted as a *c.* 1.4 Ga suture zone between the Konkiep Subprovince and the Kalahari craton (Miller 2008; 2012), although subsequent dextral offset of its continuation into the Upington region of South Africa has been estimated at about 200 km (Stowe 1983), possibly related to transform motion coincident with collision between Kalahari and other cratons during Rodinia assembly (Jacobs *et al.* 1993, 2008).

Within the Konkiep Subprovince, the Sinclair mining district is the type locality of the Sinclair Supergroup: a succession of Mesoproterozoic volcanic and sedimentary rocks dating from *c.* 1.4 to 1.1 Ga (Watters 1977; SACS 1980; Becker *et al.* 2006; Miller 2008, 2012). This stratigraphic unit continues northward around the western Kalahari cratonic promontory into the Rehoboth basement inlier at the southern margin of the Damara orogen (Becker *et al.* 2005, 2006). Recent U–Pb ages from metavolcanic and metasedimentary rocks of the Rehoboth region (Becker & Schalk 2008; Van Schijndel *et al.* 2011) have refined correlations to the less deformed and less metamorphosed strata of the Konkiep Subprovince, and conform to the model of the latter region's accretion to Kalahari as early as *c.* 1.4 Ga, as noted above. The Konkiep Group represents the entirety of the Sinclair Supergroup in the Konkiep Subprovince. Dominated by bimodal magmatism and epicontinental sedimentation (Becker *et al.* 2006), the Konkiep Group's tectonic setting has been compared with either a rift (Borg 1988) or the overriding plate of a subduction zone (Hoal 1993; Miller 2008, 2012), but the long duration of its stratigraphic accumulation probably implies a diverse range of tectonic settings. Aside from the oldest, Kairab Formation, which occupies a transitional stratigraphic position between basement and cover (Miller 2008, 2012), subsequent formations of the Konkiep Group are only mildly deformed, and greenschist-grade metamorphism is restricted to the western Awasib Mountain Terrain, which has been interpreted as a continental margin (Hoal 1993).

Five stratigraphic sequences have been recognized in the Konkiep Group (summarized by Miller 2008, 2012). The oldest, Kairab Formation, consists of bimodal metavolcanic rocks that are considered to represent island-arc magmatism prior to accretion of the Konkiep Subprovince. The remainder of the Konkiep Group comprises several cycles of siliciclastic and volcanogenic deposits, intruded by successive generations of intermediate to bimodal plutonic rocks. In the study area, these cycles are represented by mafic volcanic and volcaniclastic rocks of the Barby Formation, which is unconformably overlain by mainly medium- to coarse-grained siliciclastic sedimentary and volcanic rocks of the Guperas Formation. The Guperas Formation is in turn unconformably overlain by the Aubures Formation redbeds. The Barby Formation has been correlated with lavas in the western, Awasib Mountains, which are intruded by plutonic rocks dated by U–Pb on zircon at 1215–1220 Ma (Hoal & Heaman 1995).

The Aubures Formation is a >2600 m-thick redbed unit deposited in north–south-oriented synclinal basins, each about 40 km in length and 10 km in width (Miller 1969, 2008, 2012; Watters 1977). The western Aubures exposure forms a prominent erosional escarpment named the Rooirand ('Red

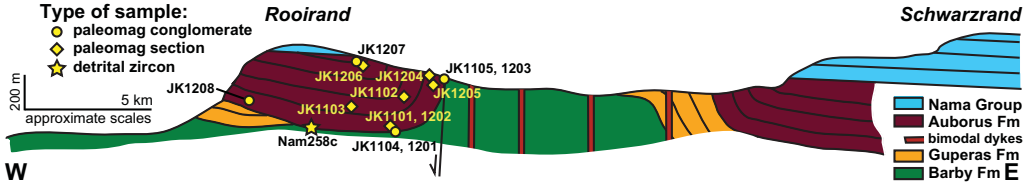


**Fig. 2.** Simplified and schematic cross-section of the Sinclair region.

Ridge'). The two Aubures outcrop areas are separated laterally by a *c.* 15 km-wide horst block, now exposed in a topographic low, containing lavas and sedimentary rocks from the underlying Barby and Guperas Formations (Fig. 2). The Aubures sediments were deposited in a shallow basin in which subsidence was contemporaneous with deposition, as evidenced by thick, coarse conglomerate facies localized to the Aubures-bounding faults adjacent to the central horst. The block faulting, concomitant with gentle folding, was entirely completed prior to deposition of the Ediacaran–Cambrian Nama Group, which once unconformably covered the entire Sinclair region. These successions are now discontinuously exposed as erosional remnants at the crest of the Rooirand, coplanar with continuous Nama exposures along the Schwarzrand ('Black Ridge') to the east (Fig. 2).

Physical sedimentary characteristics of the Aubures Formation indicate a fault-bounded alluvial–fluvial setting. The basal conglomerate facies, ranging in thickness from 360 to 1000 m (Miller 1969), is clast-supported, with subangular to subrounded clasts ranging in size from pebble to cobble. Most clasts are sourced from Barby lavas or rhyolite porphyries. Above the basal conglomerate lie arkosic, well-sorted sandstones and siltstones of varying thicknesses; grit beds are commonly interspersed. Bedding ranges in character from laminar units of decimetre order in thickness, indicating frequent inundations by shallow water, to massive beds up to 3 m thick. Locally, ripple-bedded shales are overlain by mudcracks, and rarely contain rain imprints, indicating intermittent exposure. Cross-bedding, ranging in thickness from 0.6 to 2 m, is also found throughout the formation; palaeocurrent directions and conglomerate clast compositions indicate multiple local sediment sources into the basins (Miller 1969).

## Methods

### *Palaeomagnetism*

More than 300 oriented blocks and individually oriented cores were collected through most of the thickness of the Aubures Formation to attempt a preliminary magnetostratigraphy of the succession. Blocks were oriented by magnetic compass, and cores were oriented by both magnetic and solar compasses. No significant deviation of magnetic declination from the regional average (−15 to −16°) was observed in any of the stratigraphic sections sampled.

The localities sampled in our palaeomagnetic study, all located within the Rooirand exposure area, are indicated in Figure 3. We sampled stratigraphic sections in different limbs and near the hinge of a broad, upright syncline in order to perform a fold test. Stratigraphic heights were logged for each palaeomagnetic sample in all sections. We also sampled both clasts and matrix from four conglomerates in the unit in order to apply conglomerate tests on the age palaeomagnetic remanence (Graham 1949). Although the majority of the sampled clasts are derived from pre-Aubures units – and thus, strictly speaking, the test applies to the age of remanence in those underlying formations – several clasts had similar lithologies to those of the Aubures redbeds and provided a more definitive comparison of palaeomagnetic remanence directions.

Samples were trimmed to *c.* 10 $cm^3$ specimens and analysed in the Yale Palaeomagnetic Facility using a cryogenic DC-SQuID magnetometer (sensitivity with sample holder *c.* $10^{-8}$ emu) with automated sample changer (Kirschvink *et al.* 2008). NRM measurements were followed by a low-temperature demagnetization step and about 20 successive high-temperature demagnetization steps (with controlled $N_2$ atmosphere) of decreasing intervals up to *c.* 690 °C, whereupon measured directions scattered about the origin at low intensity. Each specimen's magnetic components were resolved with principal component analysis (Kirschvink 1980) using software created by Jones (2002). Locality means, precision parameters and 95% confidence limits were calculated using Fisher (1953) statistics, inverting polarity as necessary to obtain unimodal distributions.

### *Detrital zircon geochronology*

Zircon concentrates were separated from 2–4 kg sample material at the Senckenberg Naturhistorische

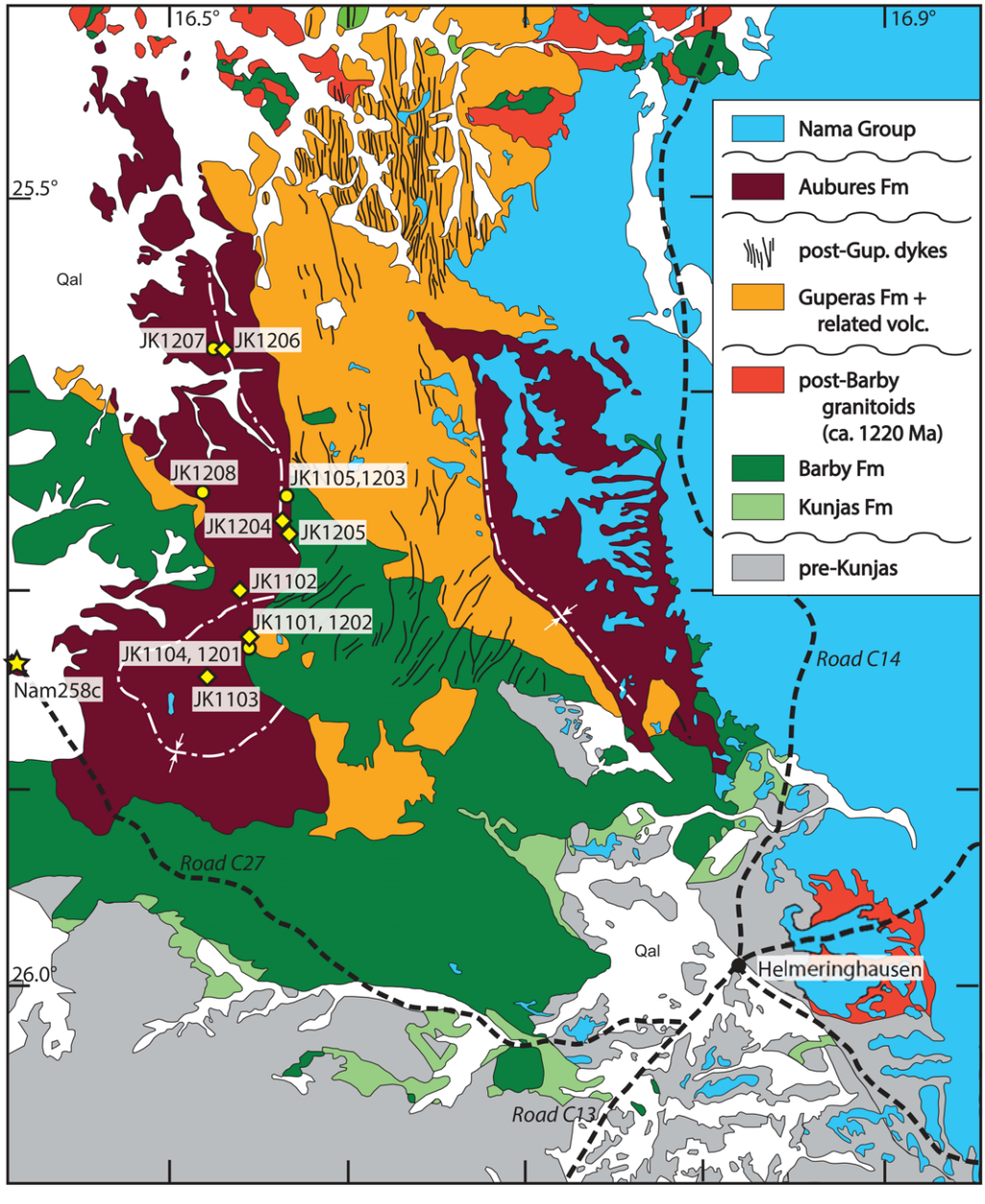


**Fig. 3.** Geological map of the Sinclair region, south-central Namibia. Sampling sites are denoted by symbols as shown in Figure 2. Dashed white line denotes synclinal axis. Qal, Quaternary alluvium.

Sammlungen Dresden (Museum für Mineralogie und Geologie) using standard methods. Final selection of the zircon grains for U–Pb dating was achieved by hand-picking under a binocular microscope. Zircon grains of all grain sizes and morphological types were selected, mounted in resin blocks and polished to half their thickness. Concerning stratigraphic ages the stratigraphic time scale of Gradstein *et al.* (2012) was used.

Laser ablation sector field inductively coupled plasma mass spectrometry (LA-SF-ICP-MS) techniques at the Museum für Mineralogie und Geologie

(GeoPlasma Laboratory, Senckenberg Naturhistorische Sammlungen Dresden), using a Thermo-Scientific Element 2 XR sector field ICP-MS coupled to a New Wave UP-193 Excimer Laser System. A teardrop-shaped, low-volume laser cell constructed by Ben Jähne (Dresden) and Axel Gerdes (Frankfurt/M.) was used to enable sequential sampling of heterogeneous grains (e.g. growth zones) during time-resolved data acquisition. Each analysis consisted of 15 s background acquisition followed by 30 s data acquisition, using a laser spot size of 25 and 35 μm, respectively. A common-Pb correction based on the interference- and background-corrected $^{204}$Pb signal and a model Pb composition (Stacey & Kramers 1975) was carried out if necessary. Raw data were corrected for background signal, common Pb, laser-induced elemental fractionation, instrumental mass discrimination and time-dependant elemental fractionation of Pb/Th and Pb/U using an Excel® spreadsheet program developed by Axel Gerdes (Institute of Geosciences, Johann Wolfgang Goethe-University Frankfurt, Frankfurt am Main, Germany). Reported uncertainties were propagated by quadratic addition of the external reproducibility obtained from the standard zircon GJ-1 (*c.* 0.6 and 0.5–1% for the $^{207}$Pb/$^{206}$Pb and $^{206}$Pb/$^{238}$U, respectively) during individual analytical sessions and the within-run precision of each analysis. Concordia diagrams ($2\sigma$ error ellipses) and concordia ages (95% confidence level) were produced using Isoplot/Ex 2.49 (Ludwig 2001) and frequency and relative probability plots using AgeDisplay (Sircombe 2004). The $^{207}$Pb/$^{206}$Pb age was taken for interpretation for all zircons $>1.0$ Ga. For further details on analytical protocol and data processing see Gerdes & Zeh (2006) and Frei & Gerdes (2009). Zircons showing a degree of concordance in the range of 90–110% in this paper are classified as concordant because of the overlap of the error ellipse with the concordia. Th/U ratios are obtained from the LA-ICP-MS measurements of investigated zircon grains. U and Pb content and Th/U ratio were calculated relative to the GJ-1 zircon standard and are accurate to approximately 10%.

## Results

### *Palaeomagnetism*

Samples from almost all of the Aubures redbeds showed excellent stability to thermal demagnetization, usually with single-component behaviour and narrow unblocking temperatures (Fig. 4), with good clustering of the characteristic remanent magnetization (ChRM) directions from each locality (Table 1, Fig. 5). Our results show broad agreement with those reported by Piper (1975), but his slightly steeper mean direction of the NRM probably resulted from contamination by a minor, unresolved overprint of the recent geomagnetic field. In our study, only at locality JK1206 was there a significant low-stability component of remanence, which was characterized by a scatter of moderately steep upward directions around that of the present local field. Apart from the dominantly N-directed ChRM polarity documented at locality JK1101/JK1202 (stratigraphically lowest), the Aubures sections have mainly south-directed, shallow ChRMs. Although our sampling did not span the Aubures Formation in its entirety, the dominance of a single magnetic polarity suggests that the majority of Aubures sedimentation occurred during a time of infrequent geomagnetic reversals.

The wide scatter of characteristic directions for clasts sampled from the four conglomerate localities (Fig. 6) indicates positive conglomerate tests, whereby magnetization can be inferred to pre-date deposition of the conglomerates. The majority of sampled clasts are igneous, typically felsic porphyries that are probably derived from the Guperas Formation or pre- or post-Guperas dykes. Two clasts from one of the tests were double-sampled in the field, and showed internally consistent ChRM directions. Six clasts are reddish sandstones that are considered to have bulk lithological properties (e.g. porosity, magnetic mineralogy) most similar to the Aubures Formation redbeds, although it is uncertain whether they derive from older Aubures horizons or sedimentary rocks of the Guperas Formation; regardless, their ChRM directions widely deviate from those of the Aubures sections. The conglomerates are geographically distributed among the sampled sections and should have experienced the same post-depositional thermochemical history. For these reasons, we consider the magnetization of the Aubures redbeds to be primary for the purposes of tectonic reconstructions.

Bedding attitudes within each locality vary only slightly, so a fold test is only possible using the combination of locality means (Table 1). Partial unfolding of the Aubures dataset is illustrated in Figure 7. Although overall precision is slightly greater at 100% tilt-corrected relative to the uncorrected data, differences in *k*-values for those two coordinate systems are statistically insignificant. There is a pronounced peak in precision at 50–60% unfolding, but given the small number of sites employed in calculating this mean, the clustering is not significantly distinct at 95% uncertainty (Fisher *et al.* 1987, p. 219). Because of evidence for deposition during basinal development as noted above, and constrained further by the positive intraformational conglomerate tests, we consider the Aubures

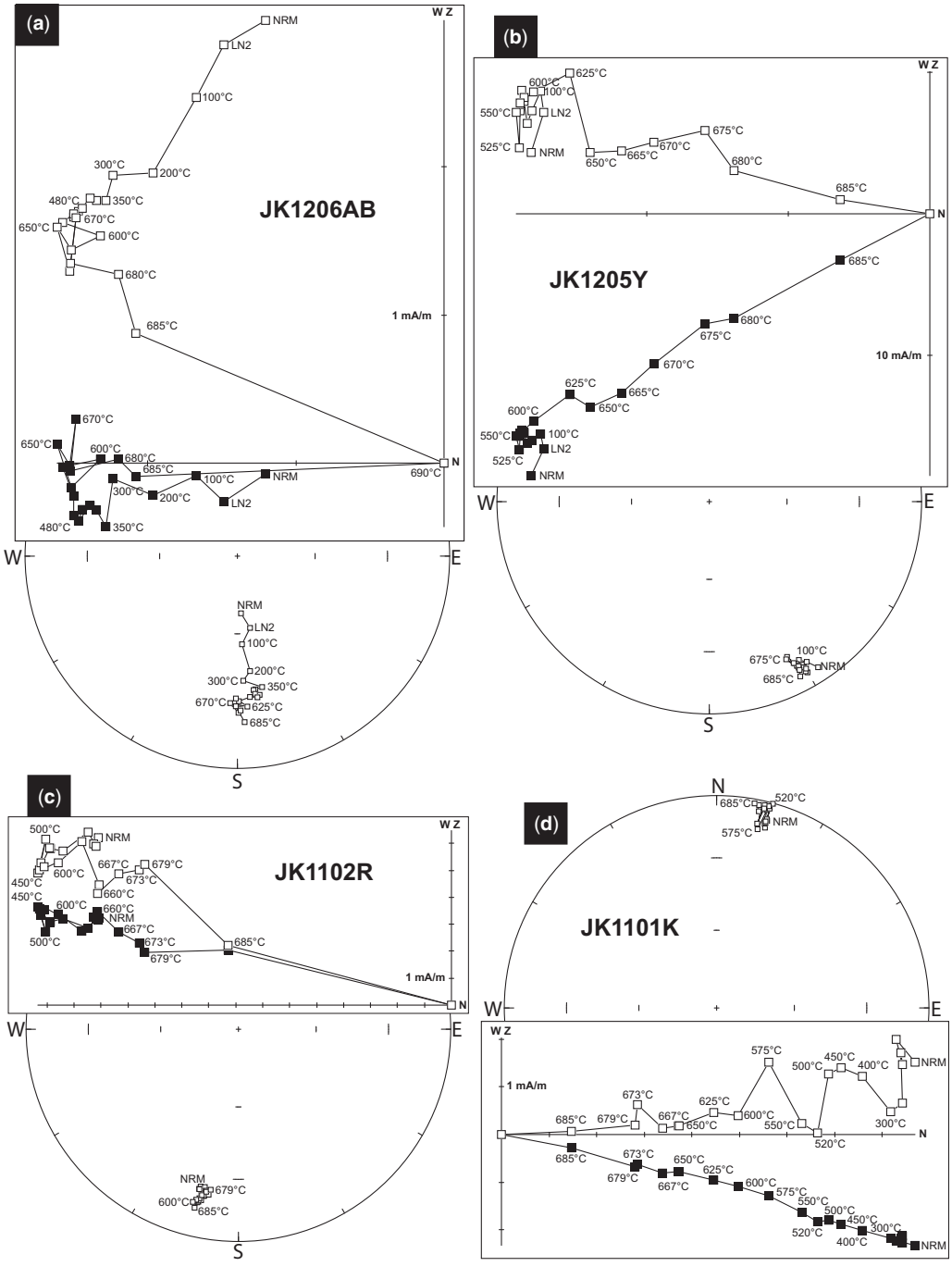


**Fig. 4.** Typical demagnetization behaviour for Aubures Formation redbeds. Panels are arranged in approximate geographic position. Each panel contains an orthogonal projection diagram, with solid v. open symbols representing the horizontal v. vertical plane, respectively. All data are shown in geographic coordinates. NRM, Natural remanent magnetization. LN2, Measurement following immersion in liquid nitrogen.

**Table 1.** *Summary of palaeomagnetic data from the Aubures Formation, Sinclair region, Namibia*

| Locality | | | Average bedding | | | | Present coordinates | | | | 100% Tilt-corrected | | | | 55% Tilt-corrected | | | | | |
|---|---|---|---|---|---|---|---|---|---|---|---|---|---|---|---|---|---|---|---|---|
| Code | Latitude (°S) | Longitude (°E) | RHS (deg) | Dip (deg) | Strat (m) | $n/N$ | $D$ (deg) | $I$ (deg) | $k$ | $\alpha_{95}$ (deg) | $D$ (deg) | $I$ (deg) | $k$ | $\alpha_{95}$ (deg) | $D$ (deg) | $I$ (deg) | $k$ | $\alpha_{95}$ (deg) | VGP latitude (°N) | VGP longitude (°E) |
| JK1101, JK1202 | 25.73 | 16.55 | 207 | 34 | 36 | 23/23 | 010.8 | 02.2 | 37.8 | 5.0 | 015.3 | −16.9 | 31.2 | 5.5 | 011.8 | −08.6 | 34.8 | 5.2 | 65.8 | 046.4 |
| JK1102 | 25.70 | 16.54 | 067 | 44 | 130 | 33/34 | 186.9 | 22.7 | 15.3 | 6.6 | 186.5 | −19.4 | 17.7 | 6.1 | 185.8 | −00.4 | 17.4 | 6.2 | 63.5 | 029.6 |
| JK1103 | 25.74 | 16.52 | 197 | 15 | 128 | 11/13 | 178.2 | −19.2 | 33.9 | 8.0 | 175.9 | −11.2 | 28.1 | 8.8 | 176.7 | −14.9 | 31.1 | 8.3 | 56.5 | 010.6 |
| JK1204 | 25.67 | 16.56 | 130 | 38 | 190 | 32/32 | 169.0 | −16.1 | 13.5 | 7.2 | 156.2 | −27.6 | 14.3 | 7.0 | 163.0 | −23.4 | 16.0 | 6.6 | 48.7 | 350.9 |
| JK1205 | 25.67 | 16.56 | 171 | 103 | 202 | 48/49 | 194.7 | −08.0 | 15.2 | 5.5 | 157.6 | −20.8 | 15.0 | 5.5 | 177.8 | −23.9 | 15.1 | 5.5 | 51.8 | 013.1 |
| JK1206 | 25.58 | 16.53 | 254 | 12 | 171 | 71/71 | 190.7 | −40.4 | 15.7 | 4.4 | 189.0 | −29.2 | 15.3 | 4.5 | 189.6 | −34.3 | 15.7 | 4.4 | 44.6 | 029.3 |
| Mean | | | | | | | 005.0 | 10.7 | 12.8 | 19.5 | 356.9 | 16.0 | 12.5 | 19.7 | 000.8 | 15.0 | 18.4 | 16.0 | 56.4 | 018.0 |
| | | | | | | | | | | | | | | | | | | | K = 36.2 | $A_{95} = 11.3°$ |

*Notes:* RHS, right-hand strike; Strat, thickness of sampled section; $n/N$, number of specimens included in the mean/number of specimens analysed; $D$, mean declination; $I$, mean inclination; $k$, $K$, Fisher's (1953) precision parameter; $\alpha_{95}$, $A_{95}$, radius of the 95% confidence cone; VGP, virtual geomagnetic pole (inverted to Northern Hemisphere as needed).

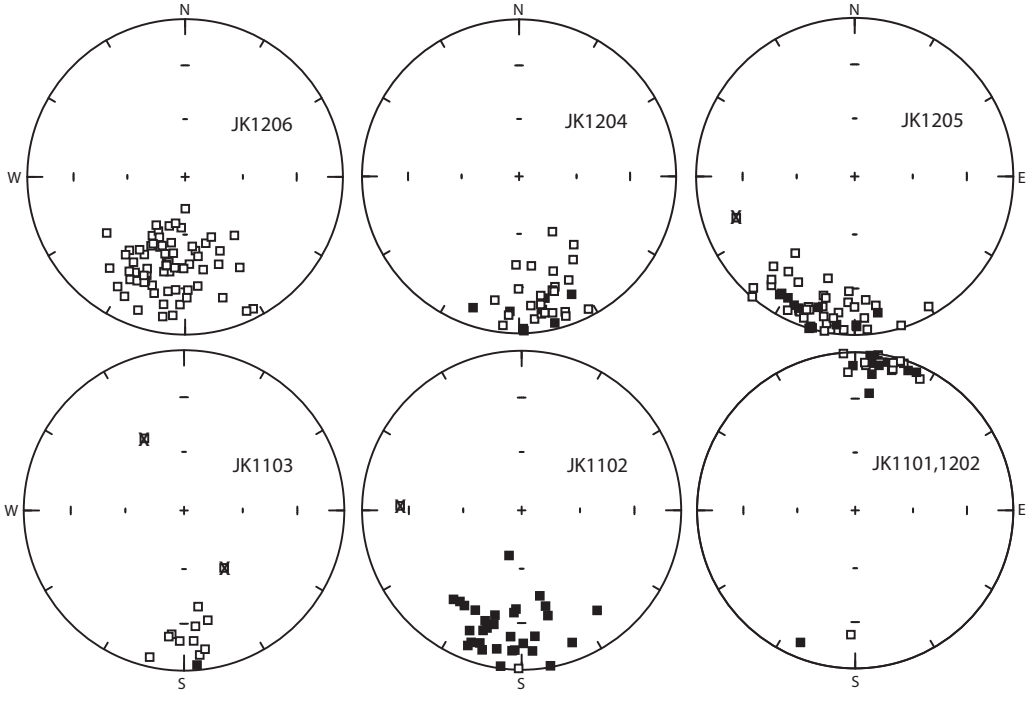


**Fig. 5.** Characteristic remanent magnetization directions, plotted on equal-area projections, from each of the Aubures section localities; all data are in geographic (0% unfolded) coordinates. Solid v. open symbols represent data on the lower v. upper hemisphere, respectively. Each 'X' marks an outlying datum that has been excluded from the mean.

palaeomagnetic remanence to be acquired during the medial stages of syndepositional tilting in the rift basins. Despite the statistical insignificance of the fold test, greatest concentration of directional data at 55% unfolding (Fig. 7) impels us to use that coordinate reference frame for our preferred mean direction. We note that this choice is inconsequential to our tectonic interpretations, as the 0, 55 and 100% site-mean directions are separated only by steps of about 5° (Table 1). The magnetization may be either a detrital remanence or an early diagenetic, chemical remanence, but in either case the data should be comparable to most palaeomagnetic results from ancient redbeds.

Using the peak directional clustering obtained upon 55% untilting of all localities, we calculate a palaeomagnetic pole at 56.4°N, 018.0°E, with statistical precision $K = 36.2$, and $A_{95} = 11.3°$ (Table 1). The implied palaeolatitude of deposition (or early diagenesis) is 08°. Our new Aubures palaeomagnetic pole largely confirms the result of Piper (1975), but raises its quality status considerably. On the Van der Voo (1990) seven-point quality scale, Piper's (1975) data satisfy only two criteria: statistics of the pole (#2) and structural control (#5). Our new result adds vector analysis (#3), positive field stability tests (#4) and dual polarity of the remanence (#6). The only criteria not yet satisfied are: a direct chronometric determination of the rock age (#1), although as shown below, there is compelling reason to suspect an age of *c.* 1100 Ma for Aubures sedimentation and magnetic remanence acquisition; and similarity to younger poles (#7), in particular the Middle Cambrian poles from Gondwana (Mitchell *et al.* 2010). Our positive field stability tests, however, render failure of that last criterion irrelevant to the reliability of the Aubures palaeomagnetic pole.

### *Detrital zircon geochronology*

Detrital zircons from the Aubures Formation yielded many concordant U–Pb data (101 out of 120 analysed), with several modes of ages ranging from 2.6 to 1.1 Ga (Fig. 8, Table 2). The largest mode, taken as a broadly distributed group, spans the 1.4–1.1 Ga interval, readily explicable in terms of the active Rehoboth and Namaqua belt margins of western Kalahari (Becker *et al.* 2006; Eglington 2006; Cornell *et al.* 2012; Miller 2012). The next mode contains just nine analyses, centred on 1.9 Ga. There are scattered analyses in the

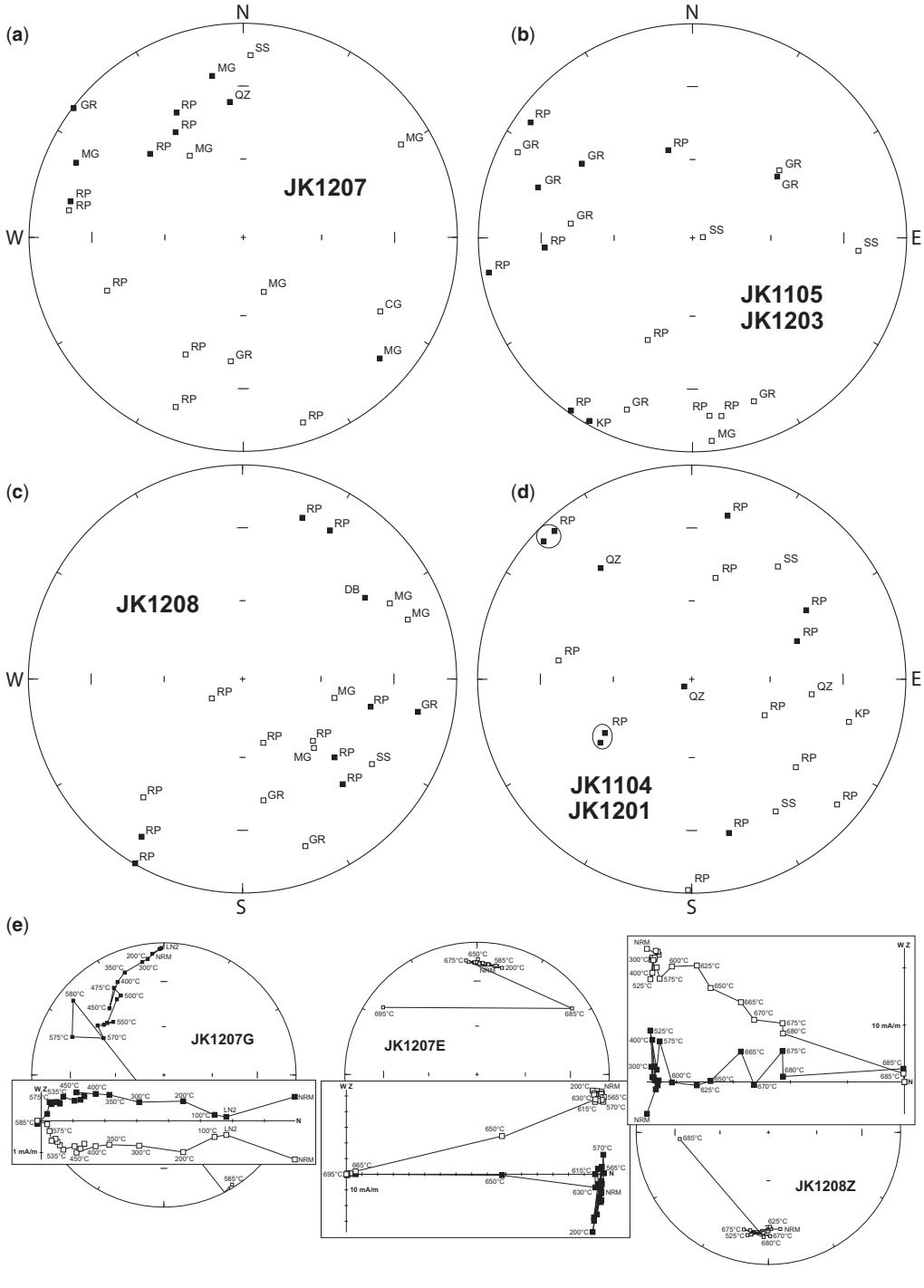


**Fig. 6.** Results of conglomerate tests in the Aubures Formation. In (A)–(D), equal-area sterographs follow the same symbol convention as in Figure 5. In (E), representative specimen demagnetization behaviours follow the same conventions as in Figure 4. Encircled pairs of data indicate double-sampled clasts for consistency tests. Abbreviations for clast lithologies: CG, onglomerate; GR, granitoid (medium-coarse grained); KP, K-feldspar porphyry; MG, microgranite/granophyre; QZ, quartzite; RP, rhyolite porphyry; SS, sandstone.

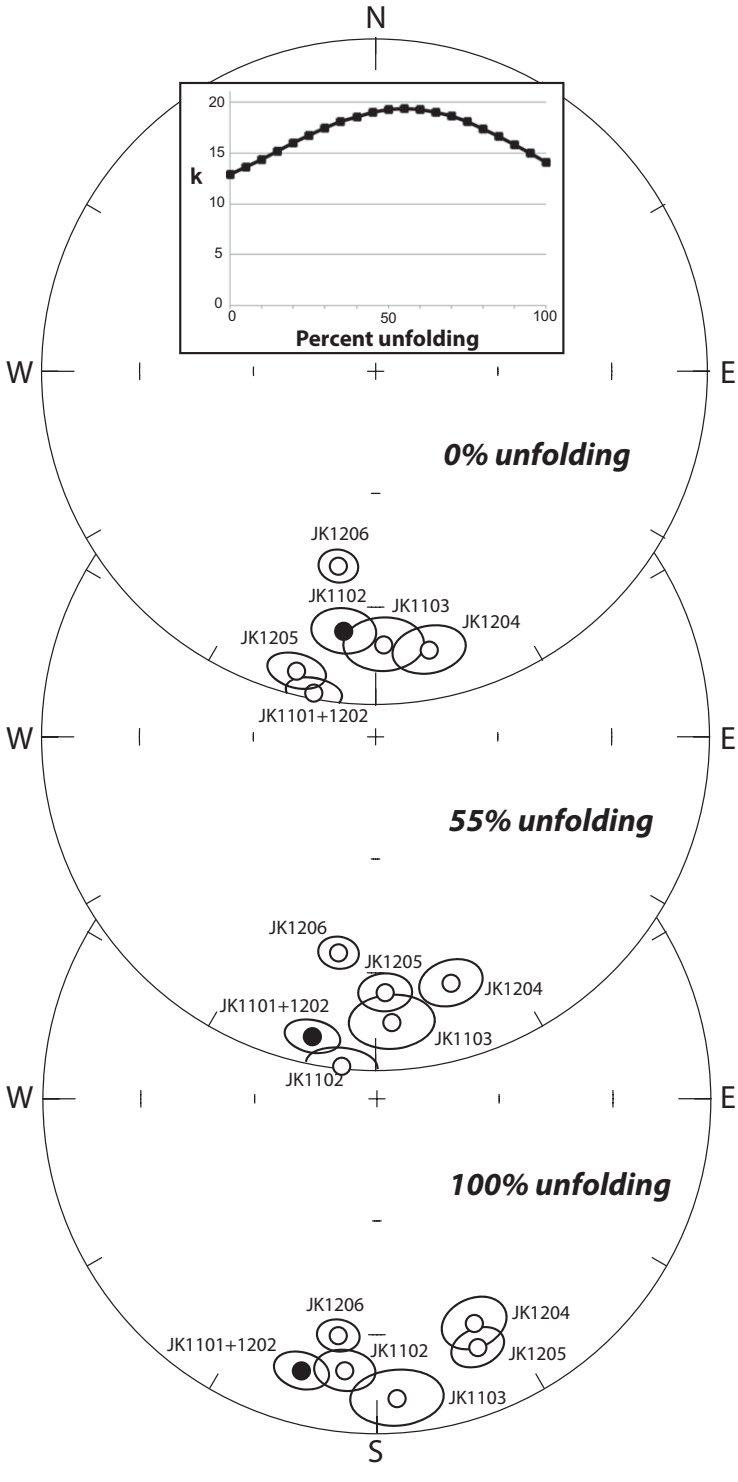


**Fig. 7.** Results of the regional fold test. Inset: Fisher's (1953) precision parameter for the mean of six locality means, according to sequential proportions of unfolding. Maximum clustering of data occurs at 55% unfolding.

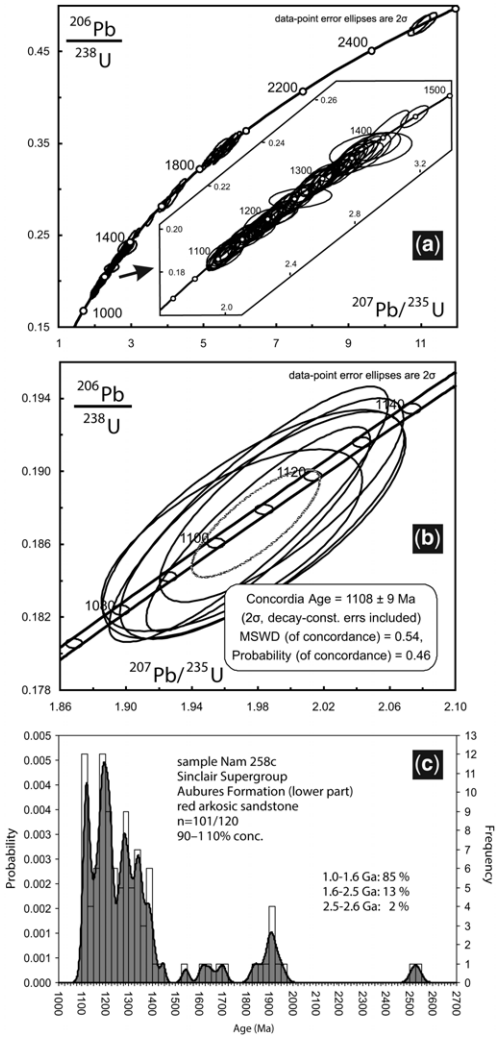


**Fig. 8.** LA-ICP-MS U–Pb ages of detrital zircon grains from the Aubures Formation. (**a**) Concordia diagram of all 90–110% concordant grains (error ellipses based on a 2$\sigma$ error level). (**b**) U–Pb concordia age of the youngest population of six detrital zircon grains providing a maximum age of sedimentation of 1108 $\pm$ 9 Ma. (**c**) Combined binned frequency and probability density distribution plots (AgeDisplay) of all concordant analyses, based on a 1$\sigma$ error level. Bin widths are 25 Ma.

1.7–1.5 Ga range, but notably, the prominent late Palaeoproterozoic (1.8–1.7 Ga) granitic magmatism in the Rehoboth basement inlier (Van Schijndel *et al.* 2014) is not represented in Aubures detritus.

Within the youngest, most prominent mode of zircon ages from the 1.4–1.1 Ga interval, submodes appear separated by about 100 myr intervals, reminiscent of the distinct magmatic pulses within the Sinclair region itself (Hoal & Heaman 1995). The youngest such pulse, represented by the six youngest analyses (a10, b9, b26, b40, b44, and b60; Table 2), yields a concordia U–Pb age of 1108 $\pm$ 9 Ma (Fig. 8b).

## Discussion

### *Correlation of redbeds across the western Kalahari craton*

Previous syntheses of the western Kalahari Mesoproterozoic geological record have emphasized the similarity of post-tectonic redbed successions from central Namibia to the Upington region of South Africa (e.g. SACS 1980; Becker *et al.* 2006; Miller 2012). The youngest population of U–Pb detrital zircon ages found in this study, with a mean of 1108 $\pm$ 9 Ma, constitutes a maximum age constraint for deposition of the Aubures Formation. In order to provide additional age constraints, the new Aubures palaeomagnetic pole is compared with the Kalahari craton's fragmental apparent polar wander (APW) path (Fig. 9, Table 3). The Aubures pole is located between poles of the Umkondo large igneous province (Gose *et al.* 2006), dated at 1112 $\pm$ 0.5 Ma to 1108 $\pm$ 0.9 Ma (Hanson *et al.* 2004) and that of the Kalkpunt Formation from the Koras Group, located near Upington, South Africa (Briden *et al.* 1979). The Kalkpunt redbeds have a maximum and probably approximate age of 1093 $\pm$ 7 Ma derived from a conformably underlying rhyolite flow (Pettersson *et al.* 2007). The Kalahari APW path migrates rapidly away from these poles towards a distant southwestern position at *c.* 1000 Ma (Gose *et al.* 2006), thus our new Aubures palaeomagnetic result suggests an age of *c.* 1100 Ma for its deposition. The new pole also supports earlier conclusions that the Sinclair succession was attached to the western margin of the Kalahari craton by at least 1100 Ma, if not substantially earlier (Becker *et al.* 2006; Miller 2012).

Proximity of our new Aubures palaeomagnetic pole to that of the Kalkpunt Formation also provides further evidence for correlation between the Konkiep Group in central Namibia, with the Koras Group in South Africa, *c.* 800 km SE (SACS 1980; Fig. 1). These successions are similar in their general profile of a deformed, metamorphosed basement being overlain by a bimodal suite of relatively undeformed volcanic rocks (Miller 2008; Bailie *et al.* 2012). Both groups contain siliciclastic metasediments, at no more than subgreenschist grade within and overlying the volcanic suite (Pettersson *et al.* 2007; Miller 2008). The groups are both found in fault-bounded basins that appear to be related to an upper-plate subduction setting

**Table 2.** *LA-SF-ICP-MS U–Pb–Th data of detrital zircon from sample Nam 258c, n = 102 of 120 analysed zircon grains; red arkosic sandstone, Aubures Formation (lower part), Sinclair Supergroup, Mesoproterozoic, roadcut NW of Helmeringhausen, Namibia, coordinates: 25°44′24.70″S; 16°24′53.90″S*

| Number | $^{207}Pb^{*}$ (cps) | (ppm) | $Pb^{\dagger}$ (ppm) | $\frac{Th^{\dagger}}{U}$ | $\frac{^{206}Pb^{\ddagger}}{^{204}Pb}$ | $\frac{^{206}Pb^{\ddagger}}{^{238}U}$ | $2\sigma$ (%) | $\frac{^{207}Pb^{\ddagger}}{^{235}U}$ | $2\sigma$ (%) | $\frac{^{207}Pb^{\ddagger}}{^{206}Pb}$ | $2\sigma$ (%) | $\rho$§ | $\frac{^{206}Pb}{^{238}U}$ | $2\sigma$ (Ma) | $\frac{^{207}Pb}{^{235}U}$ | $2\sigma$ (Ma) | $\frac{^{207}Pb}{^{206}Pb}$ | $2\sigma$ (Ma) | Concentration (%) |
|---|---|---|---|---|---|---|---|---|---|---|---|---|---|---|---|---|---|---|---|
| b60 | 5154 | 11 | 3 | 2.90 | 5408 | 0.18622 | 2.2 | 1.96416 | 3.3 | 0.07650 | 2.5 | 0.66 | 1101 | 22 | 1103 | 22 | 1108 | 49 | 99 |
| b40 | 49235 | 223 | 40 | 0.09 | 14867 | 0.18683 | 2.5 | 1.98019 | 2.8 | 0.07687 | 1.4 | 0.87 | 1104 | 25 | 1109 | 19 | 1118 | 27 | 99 |
| b9 | 8062 | 33 | 7 | 0.96 | 4637 | 0.18704 | 2.7 | 1.98256 | 3.6 | 0.07688 | 2.3 | 0.77 | 1105 | 28 | 1110 | 24 | 1118 | 45 | 99 |
| b44 | 58310 | 139 | 31 | 1.05 | 356 | 0.18710 | 2.7 | 1.97772 | 3.8 | 0.07666 | 2.6 | 0.72 | 1106 | 28 | 1108 | 26 | 1112 | 53 | 99 |
| b48 | 96998 | 226 | 46 | 0.31 | 720 | 0.18730 | 3.4 | 2.65574 | 4.8 | 0.10284 | 3.4 | 0.71 | 1107 | 35 | 1316 | 36 | 1676 | 63 | 66 |
| b26 | 141262 | 607 | 112 | 0.11 | 1329 | 0.18764 | 3.1 | 1.97445 | 3.5 | 0.07632 | 1.7 | 0.87 | 1109 | 31 | 1107 | 24 | 1103 | 35 | 100 |
| a10 | 19754 | 63 | 14 | 1.04 | 25791 | 0.18806 | 1.8 | 1.99751 | 2.4 | 0.07704 | 1.6 | 0.75 | 1111 | 19 | 1115 | 17 | 1122 | 32 | 99 |
| a12 | 6425 | 25 | 6 | 1.05 | 5482 | 0.18827 | 2.9 | 1.99350 | 3.8 | 0.07679 | 2.5 | 0.76 | 1112 | 30 | 1113 | 26 | 1116 | 49 | 100 |
| a23 | 3179 | 12 | 3 | 1.35 | 2612 | 0.18835 | 2.8 | 1.99864 | 4.6 | 0.07696 | 3.7 | 0.60 | 1112 | 29 | 1115 | 32 | 1120 | 74 | 99 |
| b13 | 20878 | 88 | 27 | 2.73 | 15453 | 0.18842 | 2.4 | 1.99446 | 3.0 | 0.07677 | 1.8 | 0.80 | 1113 | 25 | 1114 | 21 | 1115 | 36 | 100 |
| a9 | 23500 | 76 | 18 | 1.33 | 8083 | 0.18910 | 1.9 | 1.99816 | 2.8 | 0.07664 | 2.0 | 0.68 | 1116 | 20 | 1115 | 19 | 1112 | 41 | 100 |
| b46 | 44413 | 133 | 24 | 0.09 | 57706 | 0.18944 | 2.2 | 2.02907 | 2.6 | 0.07768 | 1.4 | 0.84 | 1118 | 22 | 1125 | 18 | 1139 | 27 | 98 |
| a3 | 120630 | 300 | 63 | 0.57 | 518 | 0.18952 | 2.6 | 2.01263 | 3.2 | 0.07702 | 1.9 | 0.82 | 1119 | 27 | 1120 | 22 | 1122 | 37 | 100 |
| a24 | 4311 | 16 | 5 | 2.70 | 5624 | 0.19111 | 2.3 | 2.03389 | 3.9 | 0.07718 | 3.1 | 0.60 | 1127 | 24 | 1127 | 27 | 1126 | 62 | 100 |
| a60 | 20497 | 32 | 6 | 0.33 | 8748 | 0.19141 | 2.8 | 2.04515 | 3.9 | 0.07749 | 2.7 | 0.72 | 1129 | 29 | 1131 | 27 | 1134 | 54 | 100 |
| a47 | 18379 | 49 | 9 | 0.27 | 4632 | 0.19151 | 2.4 | 2.03692 | 2.9 | 0.07714 | 1.6 | 0.83 | 1130 | 25 | 1128 | 20 | 1125 | 33 | 100 |
| b42 | 25746 | 93 | 21 | 1.02 | 1344 | 0.19171 | 2.8 | 2.04522 | 3.9 | 0.07738 | 2.7 | 0.71 | 1131 | 29 | 1131 | 27 | 1131 | 55 | 100 |
| b34 | 17871 | 87 | 18 | 0.48 | 5180 | 0.19456 | 2.8 | 2.10298 | 3.3 | 0.07839 | 1.8 | 0.85 | 1146 | 29 | 1150 | 23 | 1157 | 35 | 99 |
| b43 | 11978 | 50 | 10 | 0.58 | 15483 | 0.19575 | 2.2 | 2.11433 | 3.1 | 0.07834 | 2.1 | 0.72 | 1152 | 24 | 1153 | 22 | 1155 | 42 | 100 |
| b23 | 11076 | 46 | 10 | 0.67 | 3610 | 0.19621 | 2.4 | 2.11588 | 3.6 | 0.07821 | 2.6 | 0.67 | 1155 | 25 | 1154 | 25 | 1152 | 53 | 100 |
| a14 | 13514 | 48 | 10 | 0.49 | 15984 | 0.19617 | 2.1 | 2.13114 | 2.8 | 0.07879 | 1.9 | 0.75 | 1155 | 23 | 1159 | 20 | 1167 | 37 | 99 |
| b39 | 7013 | 29 | 6 | 0.57 | 7472 | 0.19697 | 2.4 | 2.13816 | 4.2 | 0.07873 | 3.4 | 0.57 | 1159 | 26 | 1161 | 29 | 1165 | 68 | 99 |
| b24 | 12423 | 60 | 13 | 0.77 | 11224 | 0.19715 | 2.9 | 2.13897 | 3.2 | 0.07869 | 1.5 | 0.88 | 1160 | 30 | 1161 | 23 | 1164 | 30 | 100 |
| a46 | 39827 | 99 | 19 | 0.08 | 5343 | 0.19845 | 2.0 | 2.17822 | 2.3 | 0.07961 | 1.1 | 0.87 | 1167 | 22 | 1174 | 16 | 1187 | 22 | 98 |
| a48 | 29392 | 63 | 13 | 0.54 | 12649 | 0.19845 | 1.8 | 2.17827 | 2.5 | 0.07961 | 1.7 | 0.74 | 1167 | 20 | 1174 | 17 | 1187 | 33 | 98 |
| a53 | 34792 | 70 | 15 | 0.36 | 3271 | 0.19863 | 2.4 | 2.16828 | 3.1 | 0.07917 | 1.9 | 0.79 | 1168 | 26 | 1171 | 22 | 1176 | 38 | 99 |
| b10 | 16369 | 60 | 12 | 0.48 | 7119 | 0.19872 | 2.1 | 2.18002 | 3.1 | 0.07956 | 2.3 | 0.69 | 1168 | 23 | 1175 | 22 | 1186 | 45 | 99 |
| a31 | 10176 | 35 | 9 | 1.59 | 1476 | 0.19980 | 2.1 | 2.20915 | 3.8 | 0.08019 | 3.2 | 0.55 | 1174 | 22 | 1184 | 27 | 1202 | 62 | 98 |
| b53 | 42995 | 101 | 20 | 0.21 | 2487 | 0.20005 | 2.5 | 2.18471 | 2.9 | 0.07921 | 1.4 | 0.87 | 1176 | 27 | 1176 | 20 | 1177 | 29 | 100 |
| a54 | 29197 | 55 | 12 | 0.53 | 31926 | 0.20034 | 2.3 | 2.18557 | 3.0 | 0.07912 | 1.9 | 0.78 | 1177 | 25 | 1176 | 21 | 1175 | 37 | 100 |
| b30 | 17304 | 78 | 17 | 0.83 | 10347 | 0.20088 | 2.2 | 2.20280 | 2.6 | 0.07953 | 1.4 | 0.83 | 1180 | 23 | 1182 | 18 | 1185 | 28 | 100 |
| b16 | 32812 | 127 | 26 | 0.33 | 41559 | 0.20134 | 2.4 | 2.21215 | 2.9 | 0.07969 | 1.6 | 0.82 | 1183 | 26 | 1185 | 20 | 1189 | 33 | 99 |
| b28 | 33201 | 138 | 29 | 0.41 | 14289 | 0.20144 | 2.2 | 2.21787 | 2.6 | 0.07985 | 1.3 | 0.87 | 1183 | 24 | 1187 | 18 | 1193 | 25 | 99 |
| a41 | 32773 | 85 | 17 | 0.25 | 40920 | 0.20184 | 1.8 | 2.24463 | 2.2 | 0.08066 | 1.3 | 0.82 | 1185 | 20 | 1195 | 16 | 1213 | 25 | 98 |
| b38 | 3847 | 15 | 4 | 0.91 | 4855 | 0.20306 | 2.5 | 2.22757 | 4.3 | 0.07956 | 3.5 | 0.58 | 1192 | 27 | 1190 | 31 | 1186 | 69 | 100 |

| | | | | | | | | | | | | | | | | | | | |
|---|---|---|---|---|---|---|---|---|---|---|---|---|---|---|---|---|---|---|---|
| a58 | 39122 | 50 | 11 | 0.51 | 1034 | 0.20355 | 2.6 | 2.25617 | 3.6 | 0.08039 | 2.5 | 0.72 | 1194 | 29 | 1199 | 26 | 1207 | 50 | 99 |
| a25 | 16588 | 58 | 13 | 0.72 | 2713 | 0.20343 | 2.7 | 2.25870 | 3.4 | 0.08053 | 2.0 | 0.80 | 1194 | 30 | 1200 | 24 | 1210 | 40 | 99 |
| a2 | 7931 | 22 | 5 | 0.53 | 2652 | 0.20374 | 2.1 | 2.24819 | 3.0 | 0.08003 | 2.1 | 0.70 | 1195 | 23 | 1196 | 21 | 1198 | 42 | 100 |
| a34 | 16291 | 60 | 13 | 0.60 | 5787 | 0.20392 | 2.7 | 2.26496 | 3.2 | 0.08056 | 1.8 | 0.82 | 1196 | 29 | 1201 | 23 | 1211 | 36 | 99 |
| b54 | 10076 | 25 | 5 | 0.40 | 12707 | 0.20422 | 2.2 | 2.25423 | 2.7 | 0.08006 | 1.6 | 0.82 | 1198 | 24 | 1198 | 19 | 1198 | 31 | 100 |
| b18 | 45267 | 162 | 34 | 0.33 | 56778 | 0.20630 | 2.4 | 2.28941 | 2.8 | 0.08049 | 1.4 | 0.86 | 1209 | 27 | 1209 | 20 | 1209 | 28 | 100 |
| a1 | 47265 | 139 | 27 | 0.07 | 59060 | 0.20633 | 2.0 | 2.29568 | 2.9 | 0.08069 | 2.1 | 0.69 | 1209 | 22 | 1211 | 20 | 1214 | 41 | 100 |
| a8 | 23000 | 67 | 19 | 1.89 | 20169 | 0.20672 | 2.2 | 2.29406 | 2.7 | 0.08048 | 1.5 | 0.82 | 1211 | 24 | 1210 | 19 | 1209 | 30 | 100 |
| a16 | 12219 | 42 | 11 | 1.55 | 1420 | 0.20722 | 1.7 | 2.35841 | 3.1 | 0.08254 | 2.6 | 0.56 | 1214 | 19 | 1230 | 22 | 1258 | 50 | 96 |
| a39 | 5490 | 14 | 3 | 0.57 | 3341 | 0.20732 | 2.3 | 2.34199 | 3.6 | 0.08193 | 2.8 | 0.64 | 1215 | 26 | 1225 | 26 | 1244 | 55 | 98 |
| a51 | 26315 | 52 | 15 | 1.54 | 7330 | 0.20804 | 2.0 | 2.32833 | 2.7 | 0.08117 | 1.9 | 0.74 | 1218 | 22 | 1221 | 20 | 1226 | 36 | 99 |
| a52 | 91521 | 158 | 33 | 0.21 | 1618 | 0.20811 | 3.2 | 2.32863 | 3.8 | 0.08115 | 2.0 | 0.85 | 1219 | 36 | 1221 | 27 | 1225 | 39 | 99 |
| a30 | 30019 | 101 | 22 | 0.51 | 1251 | 0.20860 | 1.8 | 2.33824 | 3.0 | 0.08129 | 2.5 | 0.58 | 1221 | 20 | 1224 | 22 | 1229 | 48 | 99 |
| b50 | 30501 | 78 | 16 | 0.25 | 4848 | 0.20966 | 2.9 | 2.34825 | 3.7 | 0.08123 | 2.2 | 0.80 | 1227 | 33 | 1227 | 26 | 1227 | 43 | 100 |
| b8 | 29649 | 97 | 22 | 0.64 | 36878 | 0.21060 | 2.3 | 2.35862 | 2.8 | 0.08123 | 1.7 | 0.80 | 1232 | 25 | 1230 | 20 | 1227 | 33 | 100 |
| a15 | 50366 | 133 | 29 | 0.37 | 2773 | 0.21248 | 2.2 | 2.44198 | 2.6 | 0.08335 | 1.3 | 0.86 | 1242 | 25 | 1255 | 19 | 1277 | 25 | 97 |
| a40 | 21742 | 54 | 12 | 0.46 | 4657 | 0.21367 | 2.4 | 2.42573 | 3.1 | 0.08234 | 2.0 | 0.77 | 1248 | 27 | 1250 | 23 | 1254 | 40 | 100 |
| b11 | 24638 | 70 | 17 | 0.75 | 29991 | 0.21389 | 2.5 | 2.44428 | 3.0 | 0.08288 | 1.7 | 0.82 | 1250 | 28 | 1256 | 22 | 1266 | 33 | 99 |
| a13 | 63126 | 171 | 48 | 1.50 | 19963 | 0.21438 | 1.8 | 2.46265 | 6.4 | 0.08331 | 6.1 | 0.28 | 1252 | 20 | 1261 | 47 | 1277 | 120 | 98 |
| b57 | 40904 | 87 | 20 | 0.57 | 2283 | 0.21453 | 2.0 | 2.49162 | 2.4 | 0.08423 | 1.3 | 0.83 | 1253 | 23 | 1270 | 17 | 1298 | 26 | 97 |
| a26 | 143124 | 429 | 95 | 0.32 | 1844 | 0.21466 | 2.5 | 2.45347 | 3.0 | 0.08290 | 1.7 | 0.83 | 1254 | 28 | 1258 | 22 | 1267 | 32 | 99 |
| a59 | 41189 | 63 | 15 | 0.65 | 23144 | 0.21583 | 1.8 | 2.48120 | 2.7 | 0.08338 | 2.0 | 0.66 | 1260 | 20 | 1267 | 19 | 1278 | 39 | 99 |
| b14 | 19701 | 58 | 16 | 1.39 | 23925 | 0.21778 | 2.7 | 2.48873 | 3.4 | 0.08288 | 2.0 | 0.80 | 1270 | 31 | 1269 | 25 | 1266 | 39 | 100 |
| a42 | 18752 | 47 | 15 | 2.03 | 6178 | 0.21873 | 2.3 | 2.51738 | 3.0 | 0.08347 | 1.9 | 0.77 | 1275 | 27 | 1277 | 22 | 1280 | 38 | 100 |
| b17 | 20478 | 69 | 15 | 0.27 | 5567 | 0.22144 | 2.3 | 2.56184 | 3.5 | 0.08391 | 2.6 | 0.67 | 1289 | 27 | 1290 | 26 | 1290 | 50 | 100 |
| a35 | 22638 | 71 | 16 | 0.32 | 1232 | 0.22192 | 2.4 | 2.56856 | 3.7 | 0.08395 | 2.8 | 0.65 | 1292 | 29 | 1292 | 28 | 1291 | 55 | 100 |
| b59 | 8583 | 16 | 4 | 1.25 | 5793 | 0.22196 | 2.2 | 2.56822 | 3.2 | 0.08392 | 2.2 | 0.71 | 1292 | 26 | 1292 | 23 | 1291 | 44 | 100 |
| b1 | 51231 | 129 | 29 | 0.16 | 2418 | 0.22273 | 2.8 | 2.58229 | 4.0 | 0.08409 | 2.8 | 0.70 | 1296 | 33 | 1296 | 29 | 1295 | 55 | 100 |
| b55 | 37361 | 72 | 17 | 0.57 | 9416 | 0.22343 | 2.4 | 2.60077 | 2.9 | 0.08442 | 1.6 | 0.83 | 1300 | 28 | 1301 | 21 | 1302 | 31 | 100 |
| a11 | 20700 | 53 | 14 | 0.94 | 17257 | 0.22358 | 2.3 | 2.61054 | 2.8 | 0.08468 | 1.7 | 0.80 | 1301 | 27 | 1304 | 21 | 1308 | 33 | 99 |
| b12 | 46239 | 149 | 34 | 0.34 | 5606 | 0.22358 | 2.0 | 2.62440 | 2.5 | 0.08513 | 1.4 | 0.82 | 1301 | 24 | 1307 | 18 | 1319 | 27 | 99 |
| a29 | 22541 | 68 | 16 | 0.34 | 26573 | 0.22425 | 2.0 | 2.65608 | 2.7 | 0.08590 | 1.7 | 0.76 | 1304 | 24 | 1316 | 20 | 1336 | 33 | 98 |
| a21 | 16675 | 45 | 11 | 0.47 | 6667 | 0.22492 | 2.6 | 2.62243 | 3.0 | 0.08456 | 1.5 | 0.87 | 1308 | 31 | 1307 | 22 | 1306 | 28 | 100 |
| a36 | 26162 | 73 | 18 | 0.51 | 30718 | 0.22620 | 2.2 | 2.67810 | 3.1 | 0.08587 | 2.1 | 0.73 | 1315 | 27 | 1322 | 23 | 1335 | 40 | 98 |
| b4 | 14350 | 41 | 10 | 0.57 | 16851 | 0.22718 | 2.7 | 2.69526 | 3.3 | 0.08605 | 2.0 | 0.80 | 1320 | 32 | 1327 | 25 | 1339 | 39 | 99 |
| b22 | 25178 | 81 | 19 | 0.46 | 29741 | 0.22856 | 2.3 | 2.68541 | 2.7 | 0.08521 | 1.4 | 0.85 | 1327 | 28 | 1324 | 20 | 1320 | 27 | 100 |
| a32 | 11778 | 41 | 10 | 0.64 | 13607 | 0.22848 | 2.8 | 2.74973 | 3.2 | 0.08728 | 1.6 | 0.86 | 1327 | 33 | 1342 | 24 | 1367 | 31 | 97 |
| b33 | 28983 | 104 | 26 | 0.66 | 34115 | 0.22919 | 2.1 | 2.70982 | 2.6 | 0.08575 | 1.5 | 0.81 | 1330 | 26 | 1331 | 20 | 1333 | 30 | 100 |
| a43 | 16852 | 40 | 10 | 0.75 | 1460 | 0.23111 | 1.9 | 2.74376 | 2.5 | 0.08611 | 1.6 | 0.77 | 1340 | 24 | 1340 | 19 | 1341 | 31 | 100 |
| b41 | 18144 | 52 | 13 | 0.74 | 21175 | 0.23103 | 2.5 | 2.75475 | 2.9 | 0.08648 | 1.5 | 0.85 | 1340 | 30 | 1343 | 22 | 1349 | 30 | 99 |
| a49 | 22533 | 39 | 11 | 0.91 | 4128 | 0.23226 | 2.5 | 2.76562 | 3.3 | 0.08636 | 2.2 | 0.76 | 1346 | 31 | 1346 | 25 | 1346 | 42 | 100 |

(*Continued*)

**Table 2.** *LA-SF-ICP-MS U–Pb–Th data of detrital zircon from sample Nam 258c, n = 102 of 120 analysed zircon grains; red arkosic sandstone, Aubures Formation (lower part), Sinclair Supergroup, Mesoproterozoic, roadcut NW of Helmeringhausen, Namibia, coordinates: 25°44′24.70″S; 16°24′53.90″S* (*Continued*)

| Number | $^{207}Pb$* (cps) | (ppm) | $Pb^{\dagger}$ (ppm) | $\frac{Th^{\dagger}}{U}$ | $\frac{^{206}Pb^{\ddagger}}{^{204}Pb}$ | $\frac{^{206}Pb^{\ddagger}}{^{238}U}$ | 2σ (%) | $\frac{^{207}Pb^{\ddagger}}{^{235}U}$ | 2σ (%) | $\frac{^{207}Pb^{\ddagger}}{^{206}Pb}$ | 2σ (%) | ρ§ | $\frac{^{206}Pb}{^{238}U}$ | 2σ (Ma) | $\frac{^{207}Pb}{^{235}U}$ | 2σ (Ma) | $\frac{^{207}Pb}{^{206}Pb}$ | 2σ (Ma) | Concentration (%) |
|---|---|---|---|---|---|---|---|---|---|---|---|---|---|---|---|---|---|---|---|
| b47 | 38797 | 84 | 21 | 0.62 | 21960 | 0.23231 | 2.2 | 2.77374 | 2.6 | 0.08660 | 1.4 | 0.85 | 1347 | 27 | 1348 | 20 | 1352 | 27 | 100 |
| b15 | 33415 | 100 | 23 | 0.26 | 11043 | 0.23302 | 2.8 | 2.82504 | 3.3 | 0.08793 | 1.8 | 0.84 | 1350 | 34 | 1362 | 25 | 1381 | 34 | 98 |
| b32 | 8658 | 32 | 8 | 0.48 | 2529 | 0.23511 | 2.2 | 2.81146 | 3.0 | 0.08673 | 2.1 | 0.71 | 1361 | 27 | 1359 | 23 | 1354 | 41 | 100 |
| a18 | 36103 | 102 | 25 | 0.53 | 1389 | 0.23516 | 1.8 | 2.86385 | 3.1 | 0.08832 | 2.5 | 0.58 | 1361 | 22 | 1372 | 24 | 1390 | 49 | 98 |
| b7 | 16024 | 37 | 12 | 1.48 | 908 | 0.23522 | 3.2 | 2.85367 | 4.7 | 0.08799 | 3.5 | 0.67 | 1362 | 39 | 1370 | 36 | 1382 | 68 | 99 |
| a38 | 15408 | 43 | 12 | 1.01 | 682 | 0.23668 | 2.8 | 2.89564 | 7.1 | 0.08873 | 6.6 | 0.39 | 1369 | 34 | 1381 | 55 | 1398 | 126 | 98 |
| a17 | 62744 | 137 | 35 | 0.48 | 1011 | 0.23751 | 1.9 | 2.87484 | 2.4 | 0.08779 | 1.4 | 0.81 | 1374 | 24 | 1375 | 18 | 1378 | 27 | 100 |
| b27 | 14855 | 51 | 14 | 0.61 | 2436 | 0.23839 | 2.2 | 2.92944 | 4.2 | 0.08912 | 3.5 | 0.53 | 1378 | 28 | 1390 | 32 | 1407 | 67 | 98 |
| b37 | 29061 | 100 | 27 | 0.78 | 6570 | 0.24165 | 4.5 | 2.94853 | 5.0 | 0.08849 | 2.1 | 0.91 | 1395 | 57 | 1394 | 39 | 1393 | 40 | 100 |
| a4 | 119896 | 230 | 65 | 0.71 | 2609 | 0.25225 | 1.6 | 3.16448 | 2.2 | 0.09098 | 1.5 | 0.75 | 1450 | 21 | 1449 | 17 | 1446 | 28 | 100 |
| b5 | 128343 | 265 | 74 | 0.38 | 2494 | 0.26677 | 2.2 | 3.52257 | 2.5 | 0.09577 | 1.3 | 0.86 | 1524 | 29 | 1532 | 20 | 1543 | 24 | 99 |
| a28 | 29826 | 64 | 20 | 0.67 | 2266 | 0.28201 | 2.0 | 3.86348 | 2.5 | 0.09936 | 1.4 | 0.82 | 1601 | 29 | 1606 | 20 | 1612 | 26 | 99 |
| a37 | 34261 | 65 | 22 | 0.85 | 6315 | 0.28429 | 2.3 | 3.95418 | 2.8 | 0.10088 | 1.6 | 0.82 | 1613 | 33 | 1625 | 23 | 1640 | 29 | 98 |
| b25 | 94403 | 268 | 81 | 0.31 | 1386 | 0.29209 | 3.5 | 4.14727 | 4.0 | 0.10298 | 1.9 | 0.87 | 1652 | 51 | 1664 | 33 | 1679 | 36 | 98 |
| a33 | 36877 | 69 | 23 | 0.67 | 29992 | 0.30363 | 2.1 | 4.36796 | 2.6 | 0.10434 | 1.5 | 0.82 | 1709 | 32 | 1706 | 21 | 1703 | 27 | 100 |
| a50 | 116016 | 111 | 38 | 0.25 | 15537 | 0.32909 | 2.1 | 5.08454 | 2.5 | 0.11206 | 1.2 | 0.87 | 1834 | 34 | 1834 | 21 | 1833 | 22 | 100 |
| b3 | 35785 | 52 | 20 | 0.73 | 21277 | 0.33413 | 2.3 | 5.22148 | 2.9 | 0.11334 | 1.6 | 0.82 | 1858 | 38 | 1856 | 25 | 1854 | 29 | 100 |
| b20 | 97314 | 156 | 55 | 0.30 | 1864 | 0.33636 | 2.2 | 5.42429 | 2.4 | 0.11696 | 0.8 | 0.94 | 1869 | 36 | 1889 | 21 | 1910 | 14 | 98 |
| b45 | 42016 | 53 | 22 | 1.13 | 36718 | 0.33868 | 2.2 | 5.38879 | 2.7 | 0.11540 | 1.4 | 0.84 | 1880 | 37 | 1883 | 23 | 1886 | 26 | 100 |
| a6 | 84739 | 97 | 38 | 0.75 | 26711 | 0.34238 | 1.7 | 5.50694 | 1.9 | 0.11666 | 0.8 | 0.90 | 1898 | 29 | 1902 | 17 | 1906 | 15 | 100 |
| a5 | 24814 | 32 | 12 | 0.63 | 2618 | 0.34427 | 2.7 | 5.53781 | 4.3 | 0.11666 | 3.4 | 0.62 | 1907 | 44 | 1906 | 37 | 1906 | 60 | 100 |
| b51 | 50216 | 52 | 21 | 0.97 | 4863 | 0.34620 | 2.3 | 5.61038 | 2.8 | 0.11753 | 1.6 | 0.83 | 1916 | 39 | 1918 | 25 | 1919 | 28 | 100 |
| b6 | 94850 | 131 | 49 | 0.41 | 9331 | 0.35063 | 2.4 | 5.73667 | 2.8 | 0.11866 | 1.5 | 0.84 | 1938 | 40 | 1937 | 25 | 1936 | 28 | 100 |
| b19 | 45008 | 60 | 26 | 1.11 | 37798 | 0.35215 | 2.4 | 5.82523 | 2.9 | 0.11997 | 1.5 | 0.84 | 1945 | 41 | 1950 | 25 | 1956 | 28 | 99 |
| a19 | 68634 | 38 | 23 | 1.02 | 41664 | 0.47824 | 1.9 | 10.94735 | 2.3 | 0.16602 | 1.3 | 0.83 | 2520 | 40 | 2519 | 22 | 2518 | 22 | 100 |
| a20 | 52408 | 32 | 20 | 1.21 | 31496 | 0.48073 | 1.9 | 11.11371 | 2.4 | 0.16767 | 1.4 | 0.81 | 2530 | 41 | 2533 | 23 | 2535 | 23 | 100 |

*Within-run background-corrected mean $^{207}Pb$ signal in counts per second.

$^{\dagger}$U and Pb content and Th/U ratio were calculated relative to GJ-1 and are accurate to approximately 10%.

$^{\ddagger}$corrected for background, mass bias, laser induced U–Pb fractionation and common Pb (if detectable, see analytical method) using Stacey & Kramers (1975) model Pb composition. $^{207}Pb/^{235}U$ calculated using $^{207}Pb/^{206}Pb/(^{238}U/^{206}Pb \times 1/137.88)$. Errors are propagated by quadratic addition of within-run errors (2SE) and the reproducibility of GJ-1 (2SD).

$^{\S}\rho$ is the error correlation defined as $err^{206}Pb/^{238}U/err^{207}Pb/^{235}$.

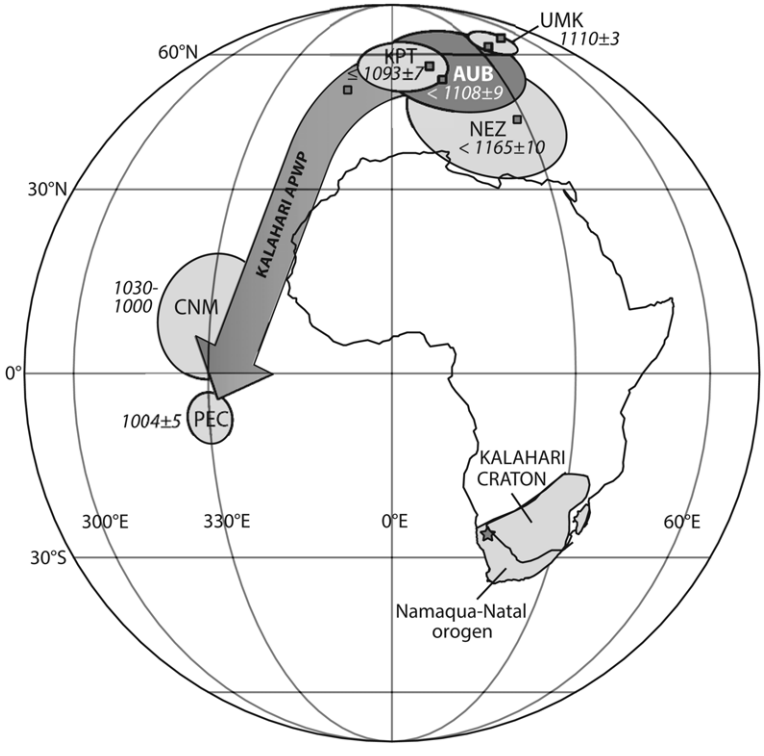


**Fig. 9.** Apparent polar wander (APW) path for the Kalahari craton between *c.* 1200 and 1000 Ma (orthographic projection). Pole codes are explained in Table 3. Small squares are the virtual geomagnetic poles (VGPs) from the six Aubures Formation locality-mean directions, each upon 55% unfolding. Ages in million years. Star, Sinclair sampling region.

characterized by alternating phases of compression and extension. Like the Aubures Formation, the Kalkpunt Formation is a red sandstone unit overlying a bimodal volcanic succession, containing a basal conglomerate as well as conglomerate lenses throughout its stratigraphy, and shale near the top of the formation. The Kalkpunt depositional environment has been interpreted as an alluvial fan developing in a synclinal structure along the fault scarps bounding the basin (SACS 1980); facies distribution was probably controlled by basement highs and syndepositional faulting, following an early Namaqua orogenic event at *c.* 1200 Ma (Gutzmer *et al.* 2000; Pettersson *et al.* 2007; Bailie *et al.* 2012). Finally, the detrital zircon age spectra from Aubures Formation, as documented in this study, are similar to the few existing U–Pb detrital zircon analyses of the Kalkpunt Formation (Pettersson *et al.* 2007). Whether or not the Konkiep and Koras basins were originally closer together, and subsequently separated by dextral motion along various NW-striking shear zones of the Namaqua Province (Stowe 1983; Miller 2012), is a question that is not resolvable by the presently available palaeomagnetic data. The Aubures and Kalkpunt poles are compatible with zero tectonic offset along Namaqua shear zones, but the 95% confidence radii of both poles would also permit relative displacement on the order of several hundred kilometers.

In the Rehoboth basement inlier, post-tectonic redbeds of the Tsumis Group include the Eskadron, Doornpoort and Klein Aub Formations, the latter hosting a significant copper deposit (Becker & Schalk 2008). They rest unconformably atop all other Rehoboth basement units, including the Langberg Formation that yielded detrital ages as young as 1103 ± 24 Ma (Van Schijndel *et al.* 2011). In fact, the Langberg and Aubures detrital zircon age populations are remarkably similar, although the Langberg strata have generally been correlated with Guperas strata based on a substantial volcanogenic component and a tectonic fabric greater than that experienced by the Aubures (Becker & Schalk 2008). Strong deformation and greenschist-facies metamorphism of the Langberg Formation at the U–Pb sampled locality (Van Schijndel *et al.* 2011) imply a post-1100 Ma tectonic event in the Rehoboth region, followed by still younger redbed

**Table 3.** *Kalahari and Sinclair palaeomagnetic poles shown in Figure 9*

| Rock name | Code | Age (Ma) | Latitude (°N) | Longitude (°E) | $A_{95}$ (deg) | 1 | 2 | 3 | 4 | 5 | 6 | 7 | Q | Reference(s) |
|---|---|---|---|---|---|---|---|---|---|---|---|---|---|---|
| Namaqua Eastern Zone | NEZ | $<1165 \pm 10$ | 45 | 022 | 13 | 0 | 1 | 1 | 1 | 0 | 0 | 0 | 3 | Evans *et al.* 2002; Pettersson *et al.* 2007 |
| Umkondo grand mean | UMK | $1110 \pm 3$ | 64 | 039 | 4 | 1 | 1 | 1 | 1 | 1 | 1 | 1 | 7 | Gose *et al.* 2006 |
| Aubures Formation | AUB | $<1108 \pm 9$ | 56 | 018 | 11 | 0 | 1 | 1 | 1 | 1 | 1 | 0 | 5 | *this study* |
| Kalkpunt Formation | KPT | $\leq 1093 \pm 7$ | 57 | 003 | 7 | 1 | 0 | 1 | 0 | 1 | 0 | 0 | 3 | Briden *et al.* 1979; Pettersson *et al.* 2007 |
| Central Namaqua belt | CNM | 1030–1000 | 08 | 330 | 10 | 1 | 1 | 1 | 0 | 0 | 1 | 0 | 4 | Onstott *et al.* 1986; Powell *et al.* 2001 |
| Port Edward Charnockite | PEC | $1004 \pm 5$ | −07 | 330 | 4 | 1 | 1 | 1 | 0 | 0 | 0 | 0 | 3 | Gose *et al.* 2004 |

*Note: Q* is the reliability factor of Van der Voo (1990).

sedimentation of the Tsumis Group. Because our Aubures palaeomagnetic pole is well constrained on the Kalahari APW path at *c.* 1100 Ma, it would appear that the Tsumis Group redbeds are younger than the Aubures and Kalkpunt Formations. Previous palaeomagnetic study of the Doornpoort redbeds, unfortunately, only identified a post-folding overprint (Piper 1975).

### *Implications for palaeogeographic reconstructions*

Because our Aubures palaeomagnetic data are comparable to existing high-quality poles from Kalahari at *c.* 1100 Ma, we add little new palaeolatitude information for use in global reconstructions during the assembly phase of the Rodinia supercontinent (cf. Li *et al.* 2008). However, the dominant magnetic polarity of our Aubures data is directed toward the south, and this may be useful for constraining orientation options for the low-latitude Kalahari craton at that time (cf. Hanson *et al.* 2004). The Aubures polarity dominance is the same as that from the Umkondo large igneous province, despite the fact that our Aubures detrital zircon data indicate deposition after Umkondo emplacement. Hanson *et al.* (2004) interpreted the south-directed, dominant Umkondo remanence as reversed polarity, but such an interpretation would imply *c.* 180° relative rotation between Kalahari

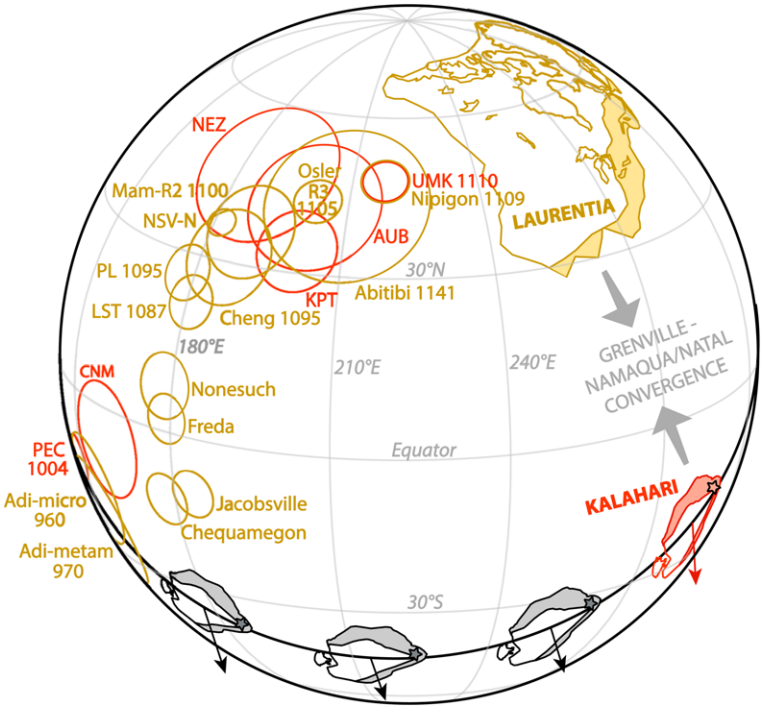


**Fig. 10.** Relative reconstruction of Kalahari and Laurentia cratons at 1110 Ma, in the present North American reference frame and orthographic projection, assuming that the dominant polarity of Aubures Formation remanence is geomagnetically Normal. The highest-quality Kalahari pole, Umkondo (Gose *et al.* 2006), is placed directly atop the coeval pole from Laurentia, Nipigon intrusions (Pisarevsky *et al.* 2014). Palaeolongitude freedom around that pole pairing allows numerous alternative locations of Kalahari (greyscale maps; present north indicated by each arrow; stars show the Sinclair region) along the 1110 Ma palaeoequator (black curve). Red Kalahari map and corresponding poles (Table 3) are restored to Laurentia (04.1°, 334.7°, −117.1°) to align, additionally, the Aubures and Kalkpunt poles with those from Laurentia at *c.* 1100 Ma, conforming to a true polar wander interpretation for the 1110–1090 Ma APW path (Swanson-Hysell *et al.* 2009). Laurentia poles: Abitibi dykes and Nipigon means (Pisarevsky *et al.* 2014), Osler R3, upper third of the Osler reversed volcanic rocks (Swanson-Hysell *et al.* 2014*a*); Mam-R2, Mamainse Point upper reversed flows (Swanson-Hysell *et al.* 2009, 2014*b*); NSV-N, North Shore Volcanics normal (Tauxe & Kodama 2009); Cheng, Chengwatana volcanics (Kean *et al.* 1997; Zartman *et al.* 1997); PL, Portage Lake volcanics (Hnat *et al.* 2006); LST, Lake Shore traps (Diehl & Haig 1994); Nonesuch (Symons *et al.* 2013), Freda (Henry *et al.* 1977), Jacobsville (Roy & Robertson 1978), Chequamegon (McCabe & Van der Voo 1983). Adi-metam, Adirondack metamorphosed anorthosites (Brown & McEnroe 2012); Adi-micro, Adirondack microcline gneisses (Brown & McEnroe 2012).

and Laurentia if the two are considered to have collided along a joint Grenville(Llano)/Namaqua–Natal suture (Dalziel *et al.* 2000; Jacobs *et al.* 2008; Loewy *et al.* 2011). As Jacobs *et al.* (2008) noted, however, the Reversed polarity interpretation for the majority of Umkondo data is merely suggestive, not definitive. The near entirety of Aubures Formation, spanning at least 1–2 km of fluvial-deltaic stratigraphy, has a south-directed palaeomagnetic remanence. Given that the Aubures contains detrital zircons as young as 1108 ± 9 Ma, and that it may correlate with the Kalkpunt Formation that is probably only slightly younger than 1093 ± 7 Ma, we suspect that an age of *c.* 1100–1090 Ma for the majority of Aubures sedimentation probably occurred during the Normal polarity (super?)chron coincident with younger Keweenawan volcanism on Laurentia.

Inverting the absolute polarity interpretation of *c.* 1100 Ma Kalahari palaeomagnetic poles carries important tectonic and palaeogeographic implications. First, it permits the Grenville (Llano) and Namaqua–Natal belts to face each other across a diminishing ocean, perhaps to collide head-on in the succeeding tens of millions of years to help build the Rodinia supercontinent (cf. Loewy *et al.* 2011). Figure 10 shows a precise superposition of the high-quality Umkondo and Nipigon intrusions poles, from Kalahari and Laurentia, respectively. By aligning just those poles, there would be freedom of palaeolongitude in Kalahari reconstructions relative to Laurentia, around a small circle about the joint palaeopole position. Four possible reconstructions of Kalahari are shown in the figure, all straddling the Umkondo palaeoequator (black curve). Second, because Laurentia and Kalahari should have lain on separate, converging plates, any similarity in the lengths and shapes of their APW paths, if not entirely fortuitous, would need to be attributed to true polar wander (TPW), which is the uniform motion of the solid Earth relative to its rotation axis. To our knowledge, Powell *et al.* (2001) were the first to suggest a TPW interpretation for the rapid continental motion implied by *c.* 1100 Ma poles from Kalahari and Laurentia, an idea thereafter incorporated into a general supercontinent-geodynamic model by Evans (2003) and quantified by Swanson-Hysell *et al.* (2009, 2014*a*) to a rate of *c.* 24 cm per year for Laurentia's palaeolatitude changes. Such rapid rates of TPW would probably dwarf contemporaneous rates of relative plate motions, thus justifying a superposition of Aubures and Kalkpunt poles atop *c.* 1100 Ma Keweenawan poles and generating our preferred (red colour) reconstruction shown in Figure 10. Agreement of the *c.* 1000 Ma poles from both cratons in the same reconstruction, however, should be coincidental, given the likely substantial convergence between Laurentia and Kalahari between 1100 and 1000 Ma (e.g. Loewy *et al.* 2011). Such a coincidence arises, according to our palaeogeographic model, because the 1000 Ma palaeomagnetic poles would have lain near the Euler stage pole of relative motion between the converging plates through that 100 myr interval.

## Conclusions

In this study, we present a new palaeomagnetic pole and new detrital zircon U–Pb data for the Mesoproterozoic Aubures Formation. U–Pb ages of zircon grains result in a maximum age of sedimentation of *c.* 1108 Ma for the Aubures Formation. The main age group of 1.4–1.1 Ga and can be explained by erosion of the Namaqua orogen along the western margin of the Kalahari craton, as well as input from the Umkondo large igneous province. Bolstered by detailed thermal demagnetization laboratory techniques, a positive intraformational conglomerate field stability test and maximal clustering of site-mean data at 55% untilting, our palaeomagnetic data demonstrate a primary magnetization that was probably contemporaneous with syndepositional folding during rift basin development. The pole overlaps with that of the Kalkpunt Formation at the top of the Koras Group in South Africa, suggesting a temporal correlation between the two redbed formations. Redbed sedimentation was widespread along the western Kalahari craton margin after the first phase of Namaqua belt orogenesis (*c.* 1200 Ma) and Umkondo large igneous province emplacement (*c.* 1110 Ma). Palaeomagnetic polarity patterns between groups of poles from Kalahari and Laurentia from *c.* 1100 Ma can help constrain global palaeogeography during Rodinia supercontinent assembly.

We thank R. Hanson and W. Gose for introducing us to the Sinclair region, J. Hessert and S. Darroch for field assistance, P. Hoffman for use of his field 'Truck Norris', and C. Hoffmann for logistical coordination with the Geological Survey of Namibia. Finally, we sincerely thank the Miller family of farm Aruab 23 for their gracious hospitality.

## References

Bailie, R., Rajesh, H. M. & Gutzmer, J. 2012. Bimodal volcanism at the western margin of the Kaapvaal Craton in the aftermath of collisional events during the Namaqua–Natal Orogeny: the Koras Group, South Africa. *Precambrian Research*, **200–203**, 163–183.

Becker, T. & Schalk, K. E. L. 2008. The Sinclair Supergroup of the Rehoboth volcanic arc from the Sossusvlei–Gamsberg area to the Gobabis region. *In*: Miller, R. McG. (ed.) *The Geology of Namibia Volume 1:*

*Archaean to Mesoproterozoic*. Ministry of Mines and Energy, Geological Survey of Namibia, Windhoek, 8-68–8-104.

Becker, T., Garoeb, H., Ledru, P. & Milesi, J.-P. 2005. The Mesoproterozoic event within the Rehoboth Basement Inlier of Namibia: review and new aspects of stratigraphy, geochemistry, structure and plate tectonic setting. *South African Journal of Geology*, **108**, 465–492.

Becker, T., Schreiber, U., Kampunzu, A. B. & Armstrong, R. 2006. Mesoproterozoic rocks of Namibia and their plate tectonic setting. *Journal of African Earth Sciences*, **46**, 112–140.

Borg, G. 1988. The Koras–Sinclair–Ghanzi rift in southern Africa. Volcanism, sedimentation, age relationships and geophysical signature of a late Middle Proterozoic rift system. *Precambrian Research*, **38**, 75–90.

Briden, J. C., Duff, B. A. & Kröner, A. 1979. Paleomagnetism of the Koras Group, Northern Cape Province. South Africa. *Precambrian Research*, **10**, 43–57.

Brown, L. L. & McEnroe, S. A. 2012. Paleomagnetism and magnetic mineralogy of Grenville metamorphic and igneous rocks, Adirondack Highlands, USA. *Precambrian Research*, **212–213**, 57–74.

Cornell, D. H., Pettersson, Å. & Simonsen, S. L. 2012. Zircon U–Pb emplacement and Nd–Hf crustal residence ages of the Straussburg Granite and Friersdale Charnockite in the Namaqua–Natal Province, South Africa. *South African Journal of Geology*, **115**, 465–484.

Dalziel, I. W. D., Mosher, S. & Gahagan, L. M. 2000. Laurentia–Kalahari collision and the assembly of Rodinia. *Journal of Geology*, **108**, 499–513.

Diehl, J. F. & Haig, T. D. 1994. A paleomagnetic study of the lava flows within the Copper Harbor Conglomerate, Michigan: new results and implications. *Canadian Journal of Earth Sciences*, **31**, 369–380.

Eglington, B. M. 2006. Evolution of the Namaqua–Natal Belt, southern Africa – a geochronological and isotope geochemical review. *Journal of African Earth Sciences*, **46**, 93–111.

Evans, D. A. D. 2003. True polar wander and supercontinents. *Tectonophysics*, **362**, 303–320.

Evans, D. A. D., Beukes, N. J. & Kirschvink, J. L. 2002. Paleomagnetism of a lateritic paleoweathering horizon and overlying Paleoproterozoic red beds from South Africa: Implications for the Kaapvaal apparent polar wander path and a confirmation of atmospheric oxygen enrichment. *Journal of Geophysical Research*, **107**, http://doi.org/10.1029/2001JB000432

Fisher, R. 1953. Dispersion on a sphere. *Proceedings of the Royal Society of London. Series A*, **217**, 295–305.

Fisher, N. I., Lewis, T. & Embleton, B. J. J. 1987. *Statistical Analysis of Spherical Data*. Cambridge University Press, Cambridge.

Frei, D. & Gerdes, A. 2009. Precise and accurate in situ U–Pb dating of zircon with high sample throughput by automated LA-SF-ICP-MS. *Chemical Geology*, **261**, 261–270.

Frimmel, H. E., Klötzli, U. & Siegfried, P. 1996. New Pb–Pb single zircon age constraints on the timing of Neoproterozoic glaciation and continental break-up in Namibia. *Journal of Geology*, **104**, 459–469.

Gerdes, A. & Zeh, A. 2006. Combined U–Pb and Hf isotope LA-(MC-) ICP-MS analysis of detrital zircons: comparison with SHRIMP and new constraints for the provenance and age of an Armorican metasediment in Central Germany. *Earth and Planetary Science Letters*, **249**, 47–61.

Gose, W. A., Johnston, S. T. & Thomas, R. J. 2004. Age of magnetization of Mesoproterozoic rocks from the Natal sector of the Namaqua–Natal belt, South Africa. *Journal of African Earth Sciences*, **40**, 137–145.

Gose, W. A., Hanson, R. E., Dalziel, I. W. D., Pancake, J. A. & Seidel, E. K. 2006. Paleomagnetism of the 1.1 Ga Umkondo large igneous province in southern Africa. *Journal of Geophysical Research*, **111**, http://doi.org/10.1029/2005JB003897

Gradstein, F. M., Ogg, J. G., Schmitz, M. D. & Ogg, G. (eds) 2012. *The Geologic Time Scale (Volumes 1 & 2)*. Elsevier, Amsterdam, 1–1083.

Graham, J. W. 1949. The stability and significance of magnetism in sedimentary rocks. *Journal of Geophysical Research*, **54**, 131–167.

Gutzmer, J., Beukes, N. J., Pickard, A. & Barley, M. E. 2000. 1170 Ma SHRIMP age for Koras Group bimodal volcanism, Northern Cape Province. *South African Journal of Geology*, **103**, 32–37.

Hanson, R. E. 2003. Proterozoic geochronology and tectonic evolution of southern Africa. *In*: Yoshida, M., Windley, B. E. & Dasgupta, S. (eds) *Proterozoic East Gondwana: Supercontinent Assembly and Breakup*. Geological Society, London, Special Publications, **206**, 427–463.

Hanson, R. E. & Crowley, J. L. *et al*. 2004. Coeval 1.1 billion year old large-scale magmatism in the Kalahari and Laurentian cratons during Rodinia supercontinent assembly. *Science*, **304**, 1126–1129.

Henry, S. G., Mauk, F. J. & Van der Voo, R. 1977. Paleomagnetism of the upper Keweenawan sediments: the Nonesuch Shale and Freda Sandstone. *Canadian Journal of Earth Sciences*, **14**, 1128–1138.

Hnat, J. S., van der Pluijm, B. A. & Van der Voo, R. 2006. Primary curvature in the Mid-Continent Rift: Paleomagnetism of the Portage Lake Volcanics (northern Michigan, USA). *Tectonophysics*, **425**, 71–82.

Hoal, B. G. 1993. The Proterozoic Sinclair Sequence in southern Namibia: intracratonic rift or active continental margin setting? *Precambrian Research*, **63**, 143–162.

Hoal, B. G. & Heaman, L. M. 1995. The Sinclair Sequence: U–Pb age constraints from the Awasib Mountain area. *Communications of the Geological Survey of Namibia*, **10**, 83–91.

Hoffman, P. F. 1991. Did the breakout of Laurentia turn Gondwanaland inside-out? *Science*, **252**, 1409–1412.

Jacobs, J., Pisarevsky, S., Thomas, R. J. & Becker, T. 2008. The Kalahari Craton during the assembly and dispersal of Rodinia. *Precambrian Research*, **160**, 142–158.

Jacobs, J. J., Thomas, R. J. & Weber, K. 1993. Accretion and indentation tectonics at the southern edge of the Kaapvaal craton during Kibaran (Grenville) orogeny. *Geology*, **21**, 203–206.

Jones, C. H. 2002. User-driven integrated software lives: 'Paleomag' paleomagnetic analysis on the

Macintosh™. *Computers and Geosciences*, **28**, 1145–1151.

Kean, W. F., Williams, I., Chan, L. & Feeney, J. 1997. Magnetism of the Keweenawan age Chengwatana lava flows, northwest Wisconsin. *Geophysical Research Letters*, **24**, 1523–1526.

Kirschvink, J. L. 1980. The least-squares line and plane and the analysis of palaeomagnetic data. *Geophys. J. Intl.*, **62**, 699–718.

Kirschvink, J. L., Kopp, R. E., Raub, T. D., Baumgartner, C. T. & Holt, J. W. 2008. Rapid, precise, and high-sensitivity acquisition of paleomagnetic and rock-magnetic data: Development of a low-noise automatic sample-changing system for superconducting rock magnetometers. *Geochemistry, Geophysics, Geosystems*, **9**, Q05Y01, http://doi.org/10.1029/2007GC001856

Li, Z. X. & Bogdanova, S. V. *et al.* 2008. Assembly, configuration, and break-up history of Rodinia: a synthesis. *Precambrian Research*, **160**, 179–210.

Li, Z.-X., Evans, D. A. D. & Halverson, G. P. 2013. Neoproterozoic glaciations in a revised global palaeogeography from the breakup of Rodinia to the assembly of Gondwanaland. *Sedimentary Geology*, **294**, 219–232.

Loewy, S. L., Dalziel, I. W. D., Pisarevsky, S., Connelly, J. N., Tait, J., Hanson, R. E. & Bullen, D. 2011. Coats Land crustal block, East Antarctica: a tectonic tracer for Laurentia? *Geology*, **39**, 859–862.

Ludwig, K. R. 2001. Users Manual for Isoplot/Ex rev. 2.49. Berkeley Geochronology Center, Berkeley, CA, Special Publications, **1a**, 1–56.

Macdonald, F. A., Strauss, J. V., Rose, C. V., Dudás, F.Ő. & Schrag, D. P. 2010. Stratigraphy of the Port Nolloth Group of Namibia and South Africa and implications for the age of Neoproterozoic iron formations. *American Journal of Science*, **310**, 862–888.

McCabe, C. & Van der Voo, R. 1983. Paleomagnetic results from the upper Keweenawan Chequamegon Sandstone: implications for red bed diagenesis and Late Precambrian apparent polar wander of North America. *Canadian Journal of Earth Sciences*, **20**, 105–112.

Miller, R. McG. 1969. The Aubures Formation of the Bethanie District, South West Africa. *Bulletin of Chamber of Mines Precambrian Research Unit*, **2**, 1–32.

Miller, R. McG. 2008. The Sinclair supergroup. *In*: Miller, R. McG. (ed.) *The Geology of Namibia Volume 1: Archaean to Mesoproterozoic*. Ministry of Mines and Energy, Geological Survey of Namibia, Windhoek, 8-1–8-67.

Miller, R. McG. 2012. Review of Mesoproterozoic magmatism, sedimentation and terrane amalgamation in southwestern Africa. *South African Journal of Geology*, **115**, 417–448.

Mitchell, R. N., Evans, D. A. D. & Kilian, T. M. 2010. Rapid early cambrian rotation of gondwana. *Geology*, **38**, 755–758.

Onstott, T. C., Hargraves, R. B. & Joubert, P. 1986. Constraints on the evolution of the Namaqua Province II: Reconnaissance palaeomagnetic and $^{40}Ar/^{39}Ar$ results from the Namaqua Province and the Kheis Belt. *Transactions of the Geological Society of South Africa*, **89**, 143–170.

Pettersson, A., Cornell, D. H., Moen, H. F. G., Reddy, S. & Evans, D. A. D. 2007. Ion-probe dating of 1.2 Ga collision and crustal architecture in the Namaqua–Natal Province of southern Africa. *Precambrian Research*, **58**, 79–92.

Piper, J. D. A. 1975. The Paleomagnetism of precambrian igneous and sedimentary rocks of the orange river belt in South Africa and South West Africa. *Geophysical Journal of the Royal Astronomical Society*, **40**, 313–344.

Pisarevsky, S. A., Elming, S.-Å., Pesonen, L. J. & Li, Z.-X. 2014. Mesoproterozoic paleogeography: supercontinent and beyond. *Precambrian Research*, **244**, 207–225.

Powell, C. McA., Jones, D. L., Pisarevsky, S. & Wingate, M. T. D. 2001. Palaeomagnetic constraints on the position of the Kalahari craton in Rodinia. *Precambrian Research*, **110**, 33–46.

Roy, J. L. & Robertson, W. A. 1978. Paleomagnetism of the Jacobsville Formation and the apparent polar path for the interval −1100 to −670 m.y. for North America. *Journal of Geophysical Research*, **83**, 1289–1304.

SACS (SOUTH AFRICAN COMMITTEE FOR STRATIGRAPHY). 1980. *Stratigraphy of South Africa: Handbook 8. Lithostratigraphy of the Republic of South Africa, South West Africa/Namibia, and the Republics of Bophuthatswana, Transkei, and Venda*. Pretoria.

Sircombe, K. N. 2004. AGE DISPLAY: an EXCEL workbook to evaluate and display univariate geochronological data using binned frequency histograms and probability density distributions. *Computers & Geosciences*, **30**, 21–31.

Stacey, J. S. & Kramers, J. D. 1975. Approximation of terrestrial lead isotope evolution by a two-stage model. *Earth & Planetary Science Letters*, **26**, 207–221.

Stowe, C. W. 1983. The Upington Geotraverse and its implications for craton margin tectonics. *In*: Botha, B. J. V. (ed.) *Namaqualand Metamorphic Complex*. Geological Society of South Africa, Special Publications, Johannesburg, **10**, 185–198.

Swanson-Hysell, N. L., Maloof, A. C., Weiss, B. P. & Evans, D. A. D. 2009. No asymmetry in geomagnetic reversals recorded by 1.1-billion-year-old Keweenawan basalts. *Nature Geoscience*, **2**, 713–717.

Swanson-Hysell, N. L., Vaughan, A. A., Mustain, M. R. & Asp, K. E. 2014*a*. Confirmation of progressive plate motion during the Midcontinent Rift's early magmatic stage from the Osler Volcanic Group, Ontario, Canada. *Geochemistry, Geophysics, Geosystems*, **15**, 2039–2047.

Swanson-Hysell, N. L., Burgess, S. D., Maloof, A. C. & Bowring, S. A. 2014*b*. Magmatic activity and plate motion during the latent stage of Midcontinent Rift development. *Geology*, **42**, 475–478.

Symons, D. T. A., Kawasaki, K. & Diehl, J. F. 2013. Age and genesis of the White Pine stratiform copper mineralization, northern Michigan, USA, from paleomagnetism. *Geofluids*, **13**, 112–126.

Tauxe, L. & Kodama, K. P. 2009. Paleosecular variation models for ancient times: clues from Keweenawan lava flows. *Physics of the Earth and Planetary Interiors*, **177**, 31–45.

Thomas, R. J., Agenbacht, A. L. D., Cornell, D. H. & Moore, J. M. 1994. The Late Kibaran of southern Africa: tectonic evolution and metallogeny. *Ore Geology Reviews*, **9**, 131–160.

Van der Voo, R. 1990. The reliability of paleomagnetic data. *Tectonophysics*, **184**, 1–9.

Van Schijndel, V., Cornell, D. H., Hoffmann, K.-H. & Frei, D. 2011. Three episodes of crustal development in the Rehoboth Province, Namibia. *In*: Van Hinsbergen, D. J. J., Buiter, S. J. H., Torsvik, T. H., Gaina, C. & Webb, S. J. (eds) *The Formation and Evolution of Africa: A Synopsis of 3.8 Ga of Earth History*. Geological Society, London, Special Publications, **357**, 27–47.

Van Schijndel, V., Cornell, D. H., Frei, D., Simonsen, S. L. & Whitehouse, M. J. 2014. Crustal evolution of the Rehoboth Province from Archaean to Mesoproterozoic times: Insights from the Rehoboth Basement Inlier. *Precambrian Research*, **240**, 22–36.

Watters, B. R. 1977. The sinclair group: definition and regional correlations. *Transactions of the Geological Society of South Africa*, **80**, 9–16.

Zartman, R. E., Nicholson, S. W., Cannon, W. F. & Morey, G. B. 1997. U–Th–Pb zircon ages of some Keweenawan Supergroup rocks from the south shore of Lake Superior. *Canadian J. Earth Sciences*, **34**, 549–561.